Light attenuation in enriched purple phototrophic bacteria cultures: Implications for modelling and reactor design

Gabriel Capson-Tojo, Damien J Batstone, Maria Grassino, Tim Hülsen

Journal Pre-proof

Light attenuation in enriched purple phototrophic bacteria cultures: implications for modelling and reactor design

Gabriel Capson-Tojo , Damien J. Batstone , Maria Grassino , Tim Hülsen

Please cite this article as: Gabriel Capson-Tojo , Damien J. Batstone , Maria Grassino , Tim Hülsen , Light attenuation in enriched purple phototrophic bacteria cultures: implications for modelling and reactor design, *Water Research* (2022), doi: https://doi.org/10.1016/j.watres.2022.118572

This is a PDF file of an article that has undergone enhancements after acceptance, such as the addition of a cover page and metadata, and formatting for readability, but it is not yet the definitive version of record. This version will undergo additional copyediting, typesetting and review before it is published in its final form, but we are providing this version to give early visibility of the article. Please note that, during the production process, errors may be discovered which could affect the content, and all legal disclaimers that apply to the journal pertain.

Light attenuation in enriched purple phototrophic bacteria cultures: implications for modelling and reactor design

Gabriel Capson-Tojo [a,b,*], Damien J. Batstone [a], Maria Grassino [a], Tim Hülsen [a]

[a] Advanced Water Management Centre, The University of Queensland, Brisbane, QLD 4072, Australia

[b] CRETUS, Department of Chemical Engineering, Universidade de Santiago de Compostela, 15782 Santiago de Compostela, Galicia, Spain

[*] Corresponding author: tel. +34 606 23 14 95, e-mail: *gabriel.capson.tojo@usc.es*

Highlights

- PPB absorb light at both NIR and VIS wavelengths

- Light scattering did not affect attenuation

- Pigments contributed considerably to attenuation via light absorption

- The proposed model (based on Lambert-Beer) represented PPB growth accurately

- Light penetration of 5 cm in concentrated cultures ($\geq$600 g VS$\cdot$m^{-3})

Graphical abstract

1

- PPB absorb light at both NIR and VIS wavelengths
- The **Lambert-Beer** law best describes attenuation
- **No** significant **scattering**
- **Pigments** responsible for most of **light losses** (absorption)
- The proposed **model** represented PPB growth **accurately**
- Light penetration of only **5 cm** in concentrated cultures
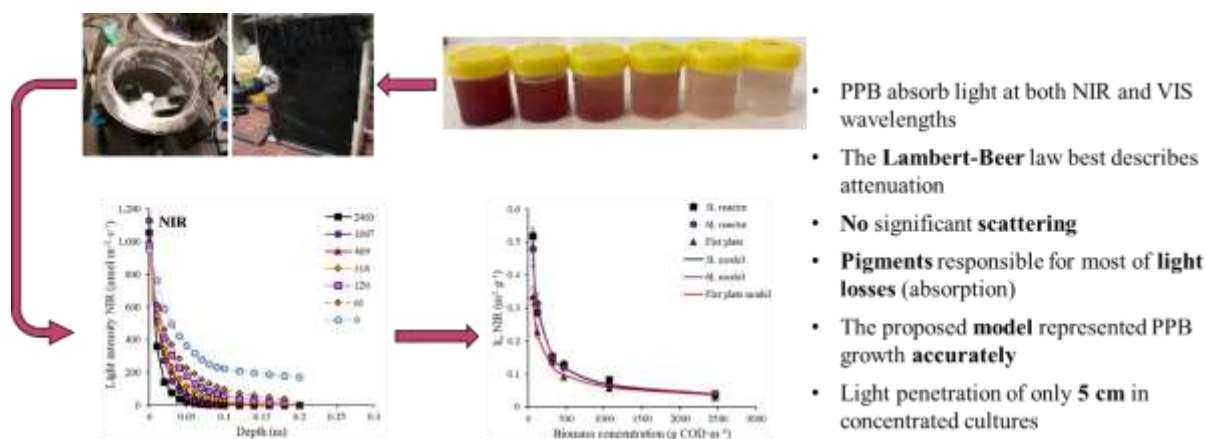
Abstract

Light attenuation in enriched purple phototrophic bacteria (PPB) cultures has not been studied, and its understanding is critical for proper process modelling and reactor design, especially for scaled systems. This work evaluated the effect of different biomass concentrations, reactor configurations, wastewater matrices, and growth conditions, on the attenuation extent of near infra-red (NIR) and ultraviolet-visible (UV-VIS) light spectra. The results show that increased biomass concentrations lead to higher light attenuation, and that PPB absorb both VIS and NIR wavelengths, with both fractions of the spectrum being equally absorbed at biomass concentrations above 1,000 g COD·m^{-3}. A flat plate configuration showed less attenuation compared with cylindrical reactors illuminated from the top, representative for open ponds. Neither a complex wastewater matrix nor the presence of polyhydroxyalkanoates (under nutrient limited conditions) affected light attenuation significantly. The pigment concentration (both bacteriochlorophyll and carotenoids) however, had a strong effect, with significant attenuation in the presence of pigments. Attenuation predictions using the Lambert-Beer law (excluding

scattering) and the Schuster model (including scattering) indicated that light scattering had a minimal effect. A proposed mathematical model, based on the Lambert-Beer law and a Monod function for light requirements, allowed effective prediction of the kinetics of photoheterotrophic growth. This resulted in a half saturation coefficient of 4.6 $W \cdot m^{-2}$. Finally, the results showed that in dense outdoor PPB cultures ($\geq 1,000$ g $COD \cdot m^{-3}$), effective light penetration is only 5 cm, which biases design away from horizontal lagoons, and towards non-incident multi-panel systems such as flat plate reactors.

Keywords

Nutrient recovery; Shading; Photoheterotrophy; Wastewater; Purple non-sulfur bacteria; Purple sulfur bacteria

Acronyms and symbols

ANOVA	Analysis of variance
ATP	Adenosine triphosphate
ASV	Amplicon sequence variant
At_{max}	Maximum attenuation observed
BChl	Bacteriochlorophyll
COD	Chemical oxygen demand
DNA	Deoxyribonucleic acid
E_a	Absorption coefficient
E_S	Scattering coefficient
FIA	Flow injection analysis
HRAP	High-rate algal pond

I_{ave}	Average light intensity
I_z	Light intensity at depth
I_0	Incident light intensity
IN	Inorganic nitrogen
IP	Inorganic phosphorus
k_a	Attenuation coefficient
Kat	Empirical constant
k_M	Maximum specific uptake rate
$k_{M,I}$	Specific uptake rate at a given light intensity
K_I	Half-saturation coefficient for light
K_S	Half-saturation coefficient
k'_a	Apparent attenuation coefficient
L	Total light path length
LED	Light-emitting diode
LHC	Light harvesting complexes
NIR	Near infrared
OD	Optical density
PAnM	Photo-anaerobic model
PAR	Photosynthetically active radiation
PBR	Photobioreactor
PFD	Photon flux density
PHA	Polyhydroxyalkanoate
PHB	Poly-β-hydroxybutyrate
PHV	Poly-β-hydroxyvalerate
PPB	Purple phototrophic bacteria

4

PWWTE	Poultry processing wastewater treatment effluent
R^2	Coefficient of determination
rRNA	Ribosomal ribonucleic acid gene
SCOD	Soluble chemical oxygen demand
SCP	Single-cell protein
TCOD	Total chemical oxygen demand
TKN	Total Kjeldahl nitrogen
TP	Total phosphorus
TS	Total solids
TSS	Total suspended solids
UV	Ultraviolet
VIS	Visible
VS	Volatile solids
VSS	Volatile suspended solids
X_{PB}	Biomass concentration
Y	Biomass yield
z	Depth

1. Introduction

Purple phototrophic bacteria (PPB) have been proposed as a potential mediator for resource recovery from wastewater, with a focus on the production of value-added products, such as polyhydroxyalkanoates (PHAs), carotenoids or biomass (*e.g.*, as single-cell protein (SCP) or fertilizer) to balance the overall costs (Capson-Tojo et al., 2020). Under anaerobic/illuminated conditions, PPB biomass is generated via anoxygenic photosynthesis, enabling the simultaneous assimilation of organics,

5

nitrogen, and phosphorus from waste streams via photoheterotrophic growth. Thanks to their ability to use light as energy source, PPB biomass yields (in terms of COD removed) close to unity can be achieved, which maximises the recovery potentials, while minimising dissipative resource losses (*e.g.*, as CO_2, N_2 or metal-bound P).

PPB transform light energy into chemical energy via light harvesting complexes (LHC) and reaction centres. LHCs are composed of bacteriochlorophylls (BChls) and a range of carotenoids. PPB utilise BChls for energy harvesting, with dominant absorbance wavelengths at over 800-900 nm, within the near infrared (NIR) spectrum (over 700 nm) (Saer and Blankenship, 2017). PPB have accessory absorption capabilities in the visible (VIS) range (around 400-700 nm) due to the presence of several carotenoids (which enable electron transfer to BChls) (Canniffe and Hunter, 2014). The utilisation of NIR wavelengths by PPB avoids the growth of other photosynthetic microbes (*e.g.*, algae and cyanobacteria) in NIR-illuminated systems, which enables effective selection and enrichment of PPB (Hülsen et al., 2018a, 2014; Madigan et al., 2011).

Despite the advantages of phototrophic processes, their inherent dependence on light also constitutes the main limiting factor in any engineered phototrophic system (Acién Fernández et al., 1997; Naderi et al., 2017). In the case of PPB, artificial illumination in large-scale systems appears economically prohibitive, and natural illumination with sunlight is the logical alternative (Capson-Tojo et al., 2020), where an efficient light supply is even more crucial, as light availability cannot be controlled. Therefore, studying light attenuation and distribution within the reactors, as well as its accurate mathematical modelling, are critical for a proper reactor design and operation (Molina Grima et al., 1999).

Decades of research have defined and partly solved the problems related to light availability in microalgae cultures (Posten, 2009). While PPB technology can profit from algae research, this knowledge cannot be directly transferred to PPB PBRs. One obvious difference between algae and PPB systems is caused by the higher water selective absorption of NIR light (see, for example, Braun and Smirnov (2020)) compared to VIS wavelengths (used by algae). At similar light paths (*e.g.*, reactor width or water column depending on the design), the PPB reactor will, a priori, have substantially less usable light than an equivalent microalgal system, as PPB preferentially use NIR wavelengths as energy source. A recent study has indeed shown that, although PPB can also use VIS wavelengths, they capability for doing so is limited, meaning that they still depend on NIR-light availability to grow efficiently (Yu et al., 2022). PPB reactors (laboratory-scale units) have also been reported to operate at higher biomass concentrations compared to traditional HRAPs (>1.0 *vs.* <0.5 $g_{biomass} \cdot L^{-1}$), which is expected to amplify shading effects and NIR attenuation via light absorption by pigments (Acién Fernández et al., 1997; Capson-Tojo et al., 2020; Robles et al., 2020b; Wagner et al., 2018). Several other aspects such as the cultivation strategy (*e.g.*, PBR *vs.* open pond, anaerobic *vs.* aerobic, or mixing strategy), reactor geometry (*e.g.*, affecting light scattering), media complexity (*e.g.*, secondary instead of tertiary treatment), and pigment concentration, can affect light attenuation.

Pigments concentration in PPB, and thus potentially light attenuation by biomass, is impacted by oxygen, which can be present either via active (aeration or turbulent mixing) or passive oxygen transfer (surface diffusion). Oxidative conditions (which can result from the presence of oxygen) are known to inhibit the expression of most genes coding for LHC and reaction centre complexes (Gregor and Klug, 1999;

Sganga and Bauer, 1992; Zhu et al., 1986), which ultimately suppresses photoheterotrophic growth, and results in pigment loss (Capson-Tojo et al., 2021).

Due to these differences compared to algal systems, the study of light attenuation and distribution within PPB reactors, as well as its accurate mathematical modelling, are critical for proper reactor design and operation. Several models have described this for algal systems, and they can also be applied for NIR behaviour. The most widely applied model to represent light attenuation is the Lambert-Beer equation (Acién Fernández et al., 1997; Marsullo et al., 2015; Ruiz-Martínez et al., 2016). This model can accurately represent light absorption in the reactors due to biomass and pigments. However, it accounts for light scattering as energy loss via absorption (neglecting the scattering of light by solids), and it has been found to lead to considerable errors in dense, concentrated, microalgae cultures (Acién Fernández et al., 1997; Wágner et al., 2018). An option to account for light scattering is the Schuster's model, adapted for cyanobacteria cultures by Cornet et al. (1992). In addition, empirical, hyperbolic models have also been applied to model attenuation in microalgae cultures, achieving accurate predictions of the light distributions (Acién Fernández et al., 1997; Naderi et al., 2017). Although other algorithms exist, such as those based on radiate transfer equations (Pilon et al., 2011), the models presented above are generally considered as the best options in terms of accuracy-simplicity compromise (Naderi et al., 2017).

The most relevant mechanistic model describing PPB growth for resource recovery from wastewater is the Photo-anaerobic model (PAnM), presented in Puyol et al. (2017). Light attenuation is not considered in this model, and the effect of light intensity is modelled following a type I approach (Béchet et al., 2013), assuming that the incident light intensity on the reactor wall is constant through the entire reactor

8

volume. A recent model for hydrogen production with PPB included light attenuation, but the conditions were different to those found in resource recovery applications (Anye Cho et al., 2021). Moreover, no experiments were conducted to estimate the relevant parameters (light intensity throughout the culture was not measured, and parameter estimation was performed for a combination of light-related parameters). While light attenuation and distribution have been extensively studied for microalgal cultures (Acién Fernández et al., 1997; Béchet et al., 2013; Naderi et al., 2017; Ruiz-Martínez et al., 2016; Wágner et al., 2018), this is missing for PPB. Therefore, the objective of this work is to determine the influence of relevant factors on light attenuation in PPB-based systems. More precisely, light attenuation was studied under different: (i) reactor configurations, (ii) biomass concentrations, (iii) wastewater matrices, (iv) growth conditions, and (v) pigment contents. In addition, different mathematical models to describe light attenuation were compared to identify the most accurate option. Experiments were also performed to determine the minimum light intensities allowing effective PPB growth. Finally, the PAnM has been modified to consider the impact of light attenuation on PPB growth.

2. Material and methods

2.1. PPB enrichments and growth media

PPB were enriched from pre-settled domestic wastewater (characteristics shown in Table S1) under anaerobic, illuminated conditions in a 2 L Schott bottle, following the procedure described in Hülsen et al. (2014). Once the typical purple colour was observed (indication for the presence of BChl and carotenoids, after around 7 days), 5 sequential dilutions were carried out to further enrich PPB, using Ormerod media (Ormerod et al., 1961) at a 1:4 inoculation ratio, and with a batch length of 3-4 days.

9

The enrichment volume increased with each dilution, obtaining eventually 30 L of enriched PPB culture (placed in three separate 10 L Schott bottles). These cultures (of 10 L each) were used for the experiments described below (Sections 2.1.1-2.1.3).

2.1.1. Further enrichment and PPB up-concentration

To further increase the PPB concentrations in the enrichments, the three 10 L bottles were re-fed three times each (as fed-batch). At the start of each fed-batch cycle (with a duration of 3-4 days) the reactors were spiked with 300 mg COD·L^{-1} of glacial acetic acid, and with the corresponding amounts of micro/macro nutrients in Ormerod media.

To further increase the biomass concentration, two of the 10 L bottles were centrifuged (10 minutes at 3,500 rpm, using an Allegra X-12 Centrifuge, Beckman Coulter) and the concentrated fraction was then mixed with the remaining 10 L enrichment (magnetic mixing was provided at 200 rpm over 2 h to ensure homogeneity). This resulted in an up-concentrated enrichment that allowed to test the attenuation effect at high total solids (TS) concentrations. The initial biomass concentration in the resulting concentrated enrichment was 2,463 g COD·m^{-3} (1.6 g VSS·L^{-1}; VSS being volatile suspended solids). This enrichment was used to generate sequential dilutions at lower TS contents (from x2 to x32 dilutions).

2.1.2. Effect of pigments on light attenuation

This experiment was designed to evaluate the impact of the presence/absence of pigments on light attenuation, and to assess the attenuation caused by the biomass itself (*e.g.*, light absorption, shading, scattering, etc.). To produce a pigment-free PPB culture (or with minimum pigment contents) a 10 L PPB enrichment (the x4 dilution from the concentrated enrichment described above) was used as inoculum for a non-illuminated, continuously aerated, enrichment (fed with Ormerod media as described

10

before, and at a 1:4 inoculation ratio). The batch lasted for 3 days, after which the typical purple colour had disappeared. Air was provided using a fine bubble aerator (60 cm Rubber Black Air Diffuser, Effosola, China) and an air compressor (Tetra Whisper 60 Air Pump, 50 $L \cdot h^{-1}$, Tetra, Germany). Total carotenoids and BChl contents were measured to confirm the pigment loss. We note that the resulting culture consisted of a mixture of PPB and aerobic heterotrophs (see Capson-Tojo et al. (2021) for typical microbial communities after aeration).

2.1.3. Effect of PHA on light attenuation

A final enrichment was carried out to determine the impact of nutrient-depleted (or excess COD) growth conditions on the light attenuation effect, mostly due to accumulation of PHA granules within the cells, which might affect light passage. For this purpose, the x4 dilution from the previous up-concentrated enrichment (Section 2.1.1) was used as inoculum for a PHA-accumulating experiment (1:4 inoculation ratio; working volume of 10 L). To maximise PHA accumulation, three sequential batch enrichment cycles were carried out as follows: (i) the cycle was started with a modified Ormerod media with reduced NH_4^+-N supply (from 107 mg $N \cdot L^{-1}$ in regular Ormerod to 30 mg $N \cdot L^{-1}$) to ensure NH_4^+-N consumption at the end of this phase, (ii) after 2 days, the enrichment was fed with extra COD as acetic acid (500 mg$\cdot L^{-1}$) to favour PHA accumulation under N-limiting conditions, (iii) on day 3, NH_4^+-N was added (at 30 mg$\cdot L^{-1}$) to select for PHA-accumulating organisms under COD limiting conditions, (iv) on day 6 the cycle was stopped, and the process was repeated, using the resulting enrichment as inoculum at a 1:4 inoculation ratio. For comparison purposes, a control reactor was carried out, fed with regular Ormerod media. Samples were taken at the end of the enrichments for determining the PHA contents.

2.1.4. Light attenuation in a real wastewater matrix

To evaluate the influence of the wastewater matrix on the attenuation effect in PPB cultures (compared to the synthetic media used in the previous experiments), the effluent from a continuous demonstration-scale PPB flat plate reactor treating poultry-processing wastewater (poultry wastewater treatment effluent; PWWTE) was also used in attenuation tests, at three different dilutions (x2, x4, and x8). An extensive characterisation of the PWWTE can be found in Table S1.

2.2. Experimental setup for attenuation assessment

To test the impact of reactor geometry on light attenuation and to represent both open ponds and flat plate reactors, the following three configurations were tested: (i) cylindrical reactor illuminated from the top (working volume of 6 L, inner and outer diameters of 16 and 17 cm, respectively, and a height of 32 cm), (ii) cylindrical reactor illuminated from the top (working volume of 3 L, inner and outer diameters of 7 and 8 cm, respectively, and a height of 81.5 cm), (iii) flat plate reactor illuminated from one side (60x41x20 cm (LxHxW), working volume of 10 L, wall thickness of 1.5 cm). All the reactors were made of Perspex, and light input from any direction other than the one desired was blocked (the cylindrical reactors were sprayed with black paint on the sides and bottom, and the flat plate was covered with black plastic foam on the bottom and all other sides but the one illuminated; the top was covered with a black high-density polyethylene cover). Pictures of the three reactors are given in the supplementary material (Figure S1).

Illumination was provided with a 150 W fluorescence lamp (Nelson Portable Flood Light; unfiltered light distribution of 17% below 700 nm, 15% at 700-800 nm, 20% at 800-900 nm and 48% at 900-1,000 nm, measured with a StellarNet BLUE-Wave Spectrometer). To measure NIR-specific light intensities, the illuminated sections of the reactors were covered with ultraviolet-visible (UV-VIS) absorbing foil (ND 1.2 299,

Transformation Tubes). To measure full-spectrum light intensities, the foil was simply removed. The UV-VIS fraction of the measured light was determined by subtracting the filtered photon flux density (PFD; $\mu mol \cdot m^{-2} \cdot s^{-1}$), consisting mostly of NIR light (98.1% of incident light above 700 nm), from the full-spectrum PFD. Total incident light intensities (on the liquid surface or the reactor wall) ranged between 1,000-1,400 $\mu mol \cdot m^{-2} \cdot s^{-1}$ (600-800 $W \cdot m^{-2}$), common values for outdoors light irradiation (Kandilli and Ulgen, 2008). This illumination strategy was followed because it represents the conditions found in outdoors PPB-enriched reactors (Hülsen et al., 2022b).

The PFD was determined using a submersible SQ-620 extended range PFD sensor (with a resolution of 0.1 $\mu mol \cdot m^{-2} \cdot s^{-1}$), measuring PFD from 340-1,050 nm, coupled to an AT-100 μcache Bluetooth micro-logger (Apogee Instruments, Inc., USA). To measure the PFD at different depths in the reactors, the base of the sensor was attached to custom-made horizontal plastic supports fixed to two magnets (Aqua One Floating Magnet Glass Cleaner, Aqua One Australia QLD, Australia), which allowed to vary the depth of the sensor. In the case of the flat plate, the distances from the light source were modified by placing the sensor on the base of a vertical metallic rod, fixed with a horizontal clamp to an external horizontal support that could be moved (see Figure S2 for pictures of the experimental set-up for PFD measurement). To ensure proper mixing of the biomass in the system and to prevent settling of solids, the reactor content was mixed between each PFD measurement, using a fine bubble aerator (60 cm Rubber Black Air Diffuser, Effosola, China) coupled to an air compressor (Tetra Whisper 60 Air Pump, 50 L per hour, Tetra, Germany). The accuracy of the experimental set-up was tested via repeating one of the tests, obtaining almost identical attenuation curves and statistically equal attenuation coefficients (p-value <0.005) (Figure S3).

13

2.3. Determination of the minimum light intensity allowing efficient photoheterotrophy

Experiments were carried out to estimate the minimum light intensity required for effective photoheterotrophic growth. To minimise attenuation, results from batch experiments using 12-well microplates (Costar, In vitro technologies pty ltd, Australia) illuminated at different light intensities (from 0-80 $W \cdot m^{-2}$) were used to estimate the kinetic parameters of Monod functions for substrate uptake. Each well had a working volume of 6.9 mL and was filled with a mixture of PPB-enriched inoculum and Ormerod media, as described in Section 2.1. Oxygen exposure was limited by covering the completely filled wells with a transparent plastic film, non-permeable to oxygen. Once filled, the microplates were placed inside custom-built closed plastic boxes. The bottoms of the boxes were equipped with NIR-specific light-emitting diodes (LED) strips (Infrared 850 nm IR LED, Waveform lighting, Vancouver, USA), which illuminated the wells. Only the NIR spectrum was considered because enriched PPB reactors are selectively illuminated with this light to allow PPB enrichment (Capson-Tojo et al., 2020). The boxes were placed inside a Thermo Scientific MaxQ400 Benchtop Orbital Shaker (Thermo Fisher Scientific, MA, USA), which was used for mixing (at 150 rpm), and for temperature control (25-27 °C). A custom-built dimmer was used to control the light intensities in the microplates. The concentrations of soluble COD (SCOD), NH_4^+-N and PO_4^{3-}-P were followed by wet analyses every 2-3 h (wells were sacrificed for this purpose). The biomass growth was estimated from optical density (OD) measurements. A more precise description of the microplate setup can be found in Grassino et al. (2022).

The maximum specific uptake rate (k_M) was estimated by minimization of the residual sum of squares, using the function lsqnonlin in Matlab (MATLAB R2018b, The MathWorks Inc., Natick, MA). 95% confidence intervals were calculated using the

14

function nlparci. A value of the half saturation constant (K_S) of 20 mg COD·L^{-1} was assumed (Puyol et al., 2017). The biomass yield (Y) was assumed as 1 g $COD_{biomass}$·g $COD_{consumed}^{-1}$ (Puyol et al., 2017). Biomass decay was considered in the model, using a first rate decay constant of 0.09 d^{-1} (Puyol et al., 2017). The resulting kinetic parameters were used as criteria to identify efficient photoheterotrophic growth (Batstone et al., 2002; Henze et al., 2000; Jeppsson et al., 2006).

The dependence of k_M on light intensity was modelled according to a Monod (substrate saturation) function (Puyol et al., 2017), of the form:

$$k_{M,I} = k_M \cdot \frac{I_{ave}}{K_I + I_{ave}} \tag{1}$$

Where, $k_{M,I}$ is the specific uptake rate at a given light intensity (d^{-1}), k_M is the maximum specific uptake rate (d^{-1}), I_{ave} is the average light intensity (W·m^{-2}), and K_I is the half-saturation coefficient for light (W·m^{-2}).

Parameter uncertainty was assessed as described in Batstone et al. (2003).

2.4. Modelling light attenuation in PPB-based systems

2.4.1. Tested models to represent light attenuation in PPB-based systems

The light attenuation due to biomass/pigments is commonly represented by the Lambert-Beer law (Equation 2):

$$I_z = I_0 \cdot e^{-k_a \cdot z \cdot X_{PB}} \tag{2}$$

Where, I_z is the light intensity (µmol·m^{-2}·s^{-1}) at depth z (m), I_0 is the incident light intensity (µmol·m^{-2}·s^{-1}), k_a is the attenuation coefficient (m^2·g^{-1}), and X_{PB} is the biomass concentration (g COD·m^{-3}). Despite its wide application, the Lambert-Beer law has been deemed as non-appropriate for high biomass concentrations, mostly because it lumps scattering with absorption, considering scattering only as a process resulting in energy loss.

15

Amongst the models considering light scattering, the Schuster's law (Equation 3) is the most popular:

$$I_z = I_0 \cdot \frac{4 \cdot \alpha}{(1+\alpha)^2 \cdot e^{\delta \cdot z \cdot X_{PB}} - (1-\alpha)^2 \cdot e^{-\delta \cdot z \cdot X_{PB}}} \qquad (3)$$

Being,

$$\alpha = \sqrt{E_a / (E_a + E_S)} \qquad (4)$$

$$\delta = \sqrt{E_a \cdot (E_a + E_S)} \qquad (5)$$

Where I_z is the light intensity ($\mu mol \cdot m^{-2} \cdot s^{-1}$) at depth z (m), I_0 is the incident light intensity ($\mu mol \cdot m^{-2} \cdot s^{-1}$), X_{PB} is the biomass concentration (g COD$\cdot m^{-3}$), E_a is the absorption coefficient (equivalent to k_a if no scattering occurs; $m^2 \cdot g^{-1}$), and E_S is the scattering coefficient (0 if no scattering occurs; $m^2 \cdot g^{-1}$).

Another option to model light attenuation is the hyperbolic empirical equation (Acién Fernández et al., 1997; Naderi et al., 2017):

$$I_z = I_0 \cdot e^{-k'_a \cdot z \cdot X_{PB}} \qquad (6)$$

$$k'_a = \frac{At_{max}}{Kat + X_{PB}} \qquad (7)$$

Where, I_z is the light intensity ($\mu mol \cdot m^{-2} \cdot s^{-1}$) at depth z (m), I_0 is the incident light intensity ($\mu mol \cdot m^{-2} \cdot s^{-1}$), k'_a is the apparent attenuation coefficient ($m^2 \cdot g^{-1}$), X_{PB} is the biomass concentration (g COD$\cdot m^{-3}$), At_{max} is the maximum attenuation observed (m^{-1}), and Kat is an empirical constant (g COD$\cdot m^{-3}$).

The coefficients corresponding to equations 2-7 were estimated for different biomass concentrations (0-2,463 g COD$\cdot m^{-3}$), enrichment conditions, reactors, and growth media. As previously, the coefficients were calculated via minimization of the sum of squares. The coefficient of determination (R^2) was used to compare between models.

2.4.2. Implementing light attenuation in mechanistic models for PPB growth

The equation from Section 2.4.1. providing the best I_z prediction was included in the

16

mechanistic PAnM, presented in Puyol et al. (2017), based on a system of ordinary differential equations and algebraic equations. Using the inhibition function and the kinetic parameters obtained from Section 2.3, the model was improved to consider light attenuation at different biomass concentrations, and a more realistic value for the light half-saturation coefficient (K_I). Matlab was used for the simulations. In the modified PAnM, once the attenuation effect was accurately predicted, the average light intensity in the growth media (along the reactor) was calculated according to Equation 8 (Béchet et al., 2013; Ruiz-Martínez et al., 2016; Wágner et al., 2016):

$$I_{ave} = \frac{1}{L}\int_0^L I_z \cdot dz \qquad (8)$$

Where, I_{ave} is the average light intensity ($W \cdot m^{-2}$), L is the total light path length (m; *e.g.* pond depth or flat plate width), I_z is the light intensity at each length step ($W \cdot m^{-2}$), and dz the different length steps (m). Assuming a properly mixed, homogeneous system, Equation 8 can represent accurately the average light that reaches each single bacterium. For unit compatibility with previous models and general measuring equipment, the resulting light intensities were converted into power density ($W \cdot m^{-2}$) according to the average energy of different spectrum fractions (different wavelengths). For the overall spectrum, a conversion factor of 2.02 $\mu mol \cdot J^{-1}$ (assuming a fraction of 45% of photosynthetically active radiation (PAR) in the broad light spectrum, and a NIR fraction of 49%) was used. For the VIS fraction a factor of 4.57 $\mu mol \cdot J^{-1}$ was applied, and for NIR wavelengths the value was 7.52 $\mu mol \cdot J^{-1}$ (Mavi and Tupper, 2004). These conversions factors imply that for an equivalent PFD, the power density of NIR wavelengths is almost halved compared to that of VIS light.

Experimental datasets from photoheterotrophic tests from Capson-Tojo et al. (2021) were used for validating the modified PAnM. The experiments consisted of batch

tests (in triplicate) carried out in 250 mL Schott bottles. The reactors were fed with domestic wastewater and spiked with acetic acid at 500 mg COD·L^{-1} to provide a readily available source of organics and to optimise the COD:N:P ratio of the media. The tests were started with 250 mL of a 1:4 vol:vol mixture of enriched PPB inoculum (1.2 ± 0.4 g VS·L^{-1}) and domestic wastewater (see Capson-Tojo et al. (2021) for details on the inoculum preparation). Each reactor was stirred at 150 rpm (RCT basic, Kika Labortechnik) and covered with UV-VIS absorbing foil (ND 1.2 299, Transformation Tubes). Continuous illumination was provided by 150 W fluorescence lamps (Nelson Portable Flood Light) at an incident intensity of 120-130 W·m^{-2} (with a distribution of 17% below 700 nm, 15% at 700-800 nm, 20% at 800-900 nm and 48% at 900-1,000 nm, measured with a StellarNet BLUE-Wave Spectrometer).

The Matlab code corresponding to the modified PAnM function, and the run file can be found in GitHub (https://github.com/GabrielCapson/PPB_Light_attenuation.git).

2.5. Analytical methods

Total COD (TCOD) and SCOD concentrations were measured using COD cell tests (Merck, 1.14541.0001, Darmstadt, Germany). TS, volatile solids (VS), total suspended solids (TSS) and VSS contents were measured according to APHA (2005). Concentrations of NH_4^+-N, NO_x-N, NO_2^--N and PO_4^{3-}-P were measured via flow injection analysis (FIA; QuikChem8000, Hach Company, Loveland, USA). Total Kjeldahl nitrogen (TKN) and total phosphorus (TP) concentrations were determined by digestion with sulphuric acid, potassium sulphate and copper sulphate, as catalysts in a block digestor (Lachat BD-46, Hach Company, Loveland, CO, USA) (Patton and Truitt, 1992). Soluble compounds were measured after filtration through a 0.45 mm membrane filter (Millipore, Millex®-HP, Merck Group, Darmstadt, Germany). The absorption spectra were measured between 300-1,100 nm, using a

18

spectrophotometer (Cary 50 conc, Varian). For determining the PHA contents, frozen samples were lyophilised (FD-1-54DD, Kinetics Thermal Systems), digested in chloroform and a 3% sulphuric acid solution in methanol (with 200 mg·L^{-1} sodium benzoate) for 20 h at 100 °C (Ratek Block Dry Digester), and analysed by GC-FID following, which allowed to identify both poly-β-hydroxybutyrate (PHB) and poly-β-hydroxyvalerate (PHV) (Oehmen et al., 2005). The pigment concentrations (BChls and total carotenoids) were determined after their extraction using a mixture of acetone/methanol (7:2 v/v), according to (Ruivo et al., 2014). After washing the samples (2.5 mL) with 2 mL of the solvent mixture, they were sonicated for 20 min (FXP14+, Unisonics Australia) and centrifuged at 3,500 rpm for 10 min. The extraction was repeated until the supernatant became clear. The resulting supernatants were collected and filtered (0.22 μm membrane filter; MF-Millipore, Merck Group, Darmstadt, Germany). All the steps were carried out under dim light conditions to prevent photooxidation. The absorbance spectrum of the pigment extract was determined using a UV-VIS spectrophotometer (Cary 50 conc, Varian). The total carotenoid and BChl contents were calculated according to the Lambert-Beer law, using the extinction coefficients given in Grassino et al. (2022).

2.6. Analysis of the microbial communities

To confirm that the present biomass was dominated by PPB, biomass samples were provided to the Australian Centre for Ecogenomics for DNA extraction and 16S rRNA gene amplicon sequencing, using the Illumina Miseq Platform. The universal primer pair 926F (50-AAACTYAAAKGAATTGACGG-30) and the 1392wR (50-ACGGGCGGTGWGTRC-30) primer sets were used (Engelbrektson et al., 2010). Raw paired reads were trimmed using Trimmomatic, to remove reads shorter that 190 bp and/or with low quality (with a Phred-33 lower than 20) (Bolger et al., 2014).

PANDAseq with default parameters was used to assemble the trimmed paired reads (Masella et al., 2012). The removal of adapter sequences was carried out using the FASTQ Clipper from the FASTX-Toolkit (Pearson et al., 1997). The resulting sequences were analysed using QIIME v1.8.0 (Caporaso et al., 2010), and were de-noised with DADA2 (Callahan et al., 2016), after which the relative frequencies of the amplicon sequence variants (ASV) were calculated. The taxonomy was assigned by uclust against the SILVA rRNA gene database (128_release) (Quast et al., 2013). ASVs with only one-two reads were filtered from the ASVs table. The resulting ASVs were processed according to Hülsen et al. (2018b).

2.7. Statistical analyses

Statistical differences were assessed via student's t tests (between final PHA contents and pigment concentrations), performed using the software R (The R Foundation, version 3.5.3). Where error bars are presented, these represent 95% confidence interval in means, from two-tailed t-tests. A 5% significance threshold was used.

3. Results and discussion

3.1. Enrichment characteristics and performance: evidence of photoheterotrophic growth and PPB dominance

Enrichments were obtained at biomass yields of 0.91 ± 0.07 g $COD_{biomass} \cdot$ g $COD_{removed}^{-1}$, and with SCOD:N:P uptake ratios of 100:10-11:2.6-3.5, values typical for photoheterotrophic growth (Capson-Tojo et al., 2020; Hülsen et al., 2014; Lu et al., 2019). The absorption spectra (Figure S4) further confirmed phototrophic growth, with the characteristic absorption peaks of PPB cultures and indicating the presence of LHCs (Capson-Tojo et al., 2021; Okubo et al., 2006; Saer and Blankenship, 2017).

20

The characteristic "purple" colour of the enrichments also showed the generation of pigments (Figure S5). The analysis of the microbial communities confirmed that PPB were dominant, with a relative abundance of 70% (over 50% of the total PPB being *Rhodopseudomonas pseudopalustris*; Figure S6). The characteristics of the produced biomass were also common for enriched PPB systems, with a COD/VSS ratio of 1.6 ± 0.2 g COD·g VSS^{-1} (90% VSS/TSS ratio), and carotenoid and BChl contents of 6.6 ± 0.5 g·g COD$_{biomass}$$^{-1}$ and 7.1 ± 1.0 g·g COD$_{biomass}$$^{-1}$, respectively (Hülsen et al., 2018a, 2014).

3.2. Light attenuation in PPB cultures

3.2.1. Effect of biomass concentration on light attenuation in different reactor configurations

The intensity of both NIR and UV-VIS fractions of the light spectra decreased at increasing light path lengths (increased distance from the light source) in all tested reactor configurations. At increasing biomass concentrations, the attenuation effect was more pronounced. Figure 1 shows the attenuation curves for the tests in the 6 L cylindrical reactor, where light intensities decreased substantially for every additional cm the light travelled, with no detectable NIR light at depths of only 5 cm for the most concentrated enrichment (2,463 g COD·m^{-3}). The obtained curves in the 3 L cylindrical reactor and the flat plate reactor were similar to those shown in Figure 1 (Figure S7).

Due to a more pronounced NIR light attenuation when compared to UV-VIS light, a negative trend in the NIR fraction was observed at increasing depths in dilute cultures (biomass concentrations of 0-469 g COD·m^{-3}; Figure 1C). Higher NIR attenuation in reactors with low biomass concentrations can be explained by the absorption of NIR wavelengths by water itself, mostly due to fundamental O-H

21

stretching vibrations (confirmed by the curves with pure water, see curves at 0 mg·L^{-1} in Figure 1 and Figure S7) (Bertie and Lan, 1996). This is highly relevant for PPB reactor design, considering that PPB utilise NIR light via BChl to grow photoheterotrophically (Saer and Blankenship, 2017). Interestingly, at high biomass concentrations (>1,000 g COD·m^{-3}) the decrease in NIR fraction with depth was not observed (Figure 1C), as the measured NIR fraction remained relatively constant at increased path lengths for all the tests at biomass concentrations above 1,000 g COD·m^{-3} (see Figures 1, S7, S9, and S10). This suggests that PPB biomass also absorbed considerable proportions of UV-VIS light. This is either due to absorbance of VIS light by carotenoids, or due to the absorbance of UV by conjugated systems (preferentially to NIR). This effect became more relevant at increased biomass concentrations and implies that, for practical purposes, both NIR and UV-VIS spectra will be absorbed equally, as biomass concentrations above 1.0 g COD$_{biomass}$·L^{-1} are commonly encountered in PPB mediated systems (Capson-Tojo et al., 2020).

The attenuation coefficients from the Lambert-Beer equation (k$_a$) were calculated for all tests. Figure 2 shows a decrease of the attenuation coefficients at higher biomass concentrations, which is in agreement with results for other phototrophic organisms, such as microalgae (Acién Fernández et al., 1997; Wágner et al., 2018). The obtained k$_a$ values all fall within the range of those reported for microalgae systems at similar biomass concentrations (after conversion to m^2·g COD^{-1} for comparison purposes; see Figure 2B) (Wágner et al., 2018). It must be mentioned that this k$_a$ values correspond to the lumped light absorption by both the solution and the biomass.

To predict the light attenuation and include this in PPB models, the dependence of the attenuation coefficients on the biomass concentrations was mathematically

represented. A power function was used for this purpose:

$$k_a = a \cdot X_{PB}{}^{-b} \tag{9}$$

Where k_a is the attenuation coefficient ($m^2 \cdot g$ COD^{-1}), X_{PB} is the biomass concentration (g COD$\cdot m^{-3}$), and a ($m^5 \cdot g^{-2}$) and b (-) are empirical parameters.

The results are presented in Figure 2 and Table 1. The defined power functions were able to precisely reproduce the observed behaviours, with R^2 values over 0.990. As the empirical coefficients were significantly different between the top-illuminated cylindrical and the side illuminated flat plate reactor, we recommend using the coefficients from the 6 L reactor for cylindrical configurations or ponds (not significantly different to those for the 3 L reactor, but with higher R^2 values and smaller confidence intervals), and those from the flat plate reactor for PBRs. The results from a global fit (combining data from all the reactors, aiming at finding a single equation), resulted in considerably higher confidence intervals and lower R^2 values. Therefore, we recommend using reactor-specific coefficients. An exponential decay relationship as presented in Wágner et al. (2018) was also tested, and did not provide an effective fit compared with the power law model (see Figure S8 and Table S2 for the results of the exponential fit).

The different attenuation behaviours between the reactor configurations can be observed in Figure 2 and Table 2, where the k_a values are presented. The k_a values confirmed that the NIR light attenuation was higher compared to UV-VIS light attenuation in all reactors, especially at biomass concentrations ≤469 g COD$\cdot m^{-3}$ (see Table S3 for k_a values for UV-VIS light). The differences between the attenuation coefficients of NIR and UV-VIS light decreased with increasing biomass concentrations (Figure S9), further confirming the UV-VIS light absorption by PPB biomass. At biomass concentrations above 1,000 g COD$\cdot m^{-3}$, k_a values for NIR light

23

were generally similar to k_a values of UV-VIS light (*e.g.*, 0.0028-0.0041 $m^2 \cdot g \; COD^{-1}$ at 2,463 $g \; COD \cdot m^{-3}$ for NIR wavelengths, and 0.0022-0.0037 $m^2 \cdot g \; COD^{-1}$ for UV-VIS light).

The reactor geometry and illumination mode (via top or side) also affected the light attenuation. While the values for the cylindrical reactors (with volumes of 3 and 6 L) were similar (overlapping curves in Figure 2), the coefficients for the flat plate were lower for any tested biomass concentration, which means that light was less attenuated. At low biomass concentrations (≤469 $g \; COD \cdot m^{-3}$), this can be explained by light reflection from the bottom and walls of the reactor, as the width of the flat plate reactor was shorter than the depth of the cylindrical reactors (see Section 2.2). This also explains why some k_a values were lower in the 6 L reactor when compared to the 3 L, at least at concentrations below 469 $g \; COD \cdot m^{-3}$ (see Table 2). It must be considered that this effect would not be observed in large scale ponds. Nevertheless, this explanation does not apply to high biomass concentrations (≥1,067 $g \; COD \cdot m^{-3}$), as light was fully attenuated before reaching the reactor wall opposed to the illuminated source (see Figures 1 and S7). Another potential explanation is an enhanced light distribution due to scattering, refraction, and diffraction in the Perspex wall of the flat plate (side illumination), which did not occur in the top-illuminated cylinders, as they were not covered with a Perspex lid (to simulate an open pond). Several other factors can explain the lower light attenuation in the flat plate reactor, such as a more even light distribution, or a higher light capture efficiency (De Vree et al., 2015). We note that additional tests with a 1.5 cm thick Perspex sheet over the flat plate reactor wall (total thickness of 2.5 cm) were performed to simulate a thicker reactor wall. The results showed that increasing the wall thickness did not significantly affect the observed attenuation curves or the k_a values (results not

24

shown).

The differences between the reactors configurations are more obvious when looking at the effective attenuation coefficients, defined as $k_a \cdot X_{PB}$ (Wágner et al., 2018). As a consequence of increased light attenuation, the effective attenuation coefficients increased at higher biomass concentrations (Figure 3). Nevertheless, the values were always lower for the flat plate reactor, regardless of the biomass concentration or the region of the light spectrum tested. More research must be carried to elucidate the precise reasons behind this finding.

3.2.2. Effect of wastewater matrix and growing conditions on light attenuation

The results corresponding to the experiments performed to evaluate the impact of additional factors (other than the biomass concentration itself) on light attenuation in PPB cultures are shown in Figure 4. Amongst the tested factors (*i.e.*, wastewater matrix, PHA content, and presence of pigments), the single one that had a significant impact on light attenuation was the presence of pigments (*i.e.*, BChl and carotenoids).

The impact of the wastewater matrix was studied using the effluent from a continuous demonstration-scale PPB flat plate reactor treating poultry-processing wastewater (poultry wastewater treatment effluent; PWWTE), in the 6 L cylindrical reactor. The corresponding k_a values, presented in Figures 4A-B, show that the attenuation effect was practically identical between synthetic media and PWWTE (despite the considerable quantity of solids contained in the wastewater (Table S1); see Table S4 for the corresponding attenuation coefficients for different models).

This was also observed when comparing a PPB culture with increased PHA contents (grown under nutrient deficiency), with a control grown with full nutrient supply (the corresponding PHA contents were 113 ± 35 mg PHA·g $VSS_{biomass}^{-1}$ in the PHA-

enriched culture and 35 ± 11 g PHA·g $VSS_{biomass}^{-1}$ in the nutrient supplied control, Figure S10). The k_a curves for the PHA-enriched culture (Figures 4C-D) show that higher PHA contents within the biomass did not affect light attenuation (attenuation curves and k_a values can be found in Figure S11 and Table S4). These results are highly relevant when considering that most of the research on PPB application to date has been carried out for hydrogen production, under nutrient limitations (commonly N), which results in simultaneous PHA accumulation within the cells (Capson-Tojo et al., 2020; Ghimire et al., 2015). In addition, as the concentrations of pigments were not significantly different between the PHA-enriched culture and the control reactor (see Figure S10), this experiment also served to confirm that, unlike microalgae do with chlorophylls, PPB do not consume BChl as N source under nutrient-deprived conditions (Wágner et al., 2018). This is highly relevant, as pigments such as BChl have a considerable impact on light attenuation.

Indeed, as opposed to the PWWTE and the PHA tests, the presence of pigments (*i.e.*, carotenoids and BChls) did affect light attenuation. After suppressing pigment synthesis and reducing their concentrations (by oxidation) via continuous aeration as in Capson-Tojo et al. (2021) (from 5.68-6.63 mg carotenoids·g $COD_{biomass}^{-1}$ and 5.8-7.1 mg BChl·g $COD_{biomass}^{-1}$ in anaerobic enrichments to 0.45 ± 0.08 mg carotenoids·g $COD_{biomass}^{-1}$ and 0.52 ± 0.06 BChl mg·g $COD_{biomass}^{-1}$ after aeration, see Figure S10), the k_a values were basically halved in the non-pigmented culture (Figures 4E-F). The different light attenuation behaviour between the anaerobic-pigmented enrichments and the non-pigmented culture becomes even more evident when looking at the corresponding effective attenuation coefficients ($k_a \cdot X_{PB}$; shown in Figure S12). The impact of the pigment concentration on the k_a values further suggests that light absorption by pigmented biomass (rather than scattering) is the

26

major factor affecting light attenuation. The attenuation curves and k_a values for these tests are shown in Figure S13 and Table S4.

In summary, both the PWWTE and the PHA-enriched tests suggest that the parameters presented in Tables 1 and 2 can be extrapolated to represent light attenuation in real applications, using complex wastewaters, and/or under conditions prone to induce PHA accumulation. This does not apply to colourless PPB cultures (*e.g.*, aerated and grown under oxidative conditions), as the pigment content was the only variable amongst the tested that significantly affected the extent of light attenuation. For all the tests presented above, the corresponding effective attenuation coefficients further confirmed the obtained results (see Figure S12).

3.3. Modelling light availability in PPB cultures

3.3.1. Selecting a simple light attenuation model for enriched PPB-cultures

Three different modelling approaches (*i.e.*, Lambert-Beer law, Schuster's law, and a hyperbolic empirical equation) were tested to find the option that allowed the best prediction of light attenuation in enriched PPB cultures. The results for NIR wavelengths in the three reactor configurations tested using cultures grown on synthetic media are shown in Table 2 (results for UV-VIS wavelengths can be found in Table S3, and those for the PWWTE, the PHA-enriched culture, and the pigment-free test (from Section 3.2.2) are presented in Table S4). The performance of the three tested models was the same at all tested conditions (same R^2 values). The first conclusion to draw from this is that light scattering did not affect light attenuation in the reactors. The facts that the values of k_a from Lambert-Beer were at all the conditions equal to E_a from the Schuster's law, and that the E_S values (term accounting for light scattering) were basically always zero (all values below 10^{-3} and most below 10^{-6}), confirm that scattering had little or no impact in any of the tests

performed. This is in agreement with the results from the non-pigmented tests, confirming that light absorption by cells (not refraction or scattering) was the predominant mechanism affecting attenuation. This lack of scattering is opposed to most of the literature on microalgae, where light scattering was found to have a significant effect of light attenuation, and where the application of the Lambert-Beer law has been found to lead to considerable errors in dense, concentrated, microalgae cultures (Acién Fernández et al., 1997; Naderi et al., 2017; Wágner et al., 2018). Multiple reasons can explain the different behaviour in PPB cultures, including the absence of bubbles (no aeration), a more efficient light utilisation, higher energy dissipation as heat, smaller cell sizes, and/or higher pigments contents. Using the empirical hyperbolic equation did not improve the prediction performance either. In addition, the value of At_{max} (with a confidence interval of 0, thus defining the model) was equal to $K_a \cdot X_{PB}$ (the effective attenuation coefficient derived from the Lambert-Beer law) in all the tested conditions, suggesting that the Lambert-Beer equation was able to predict the light attenuation to the same extent as the hyperbolic equation.

Overall, we recommend the use of the Lambert-Beer law to model light attenuation in enriched PPB cultures, as light absorption by pigmented biomass is the main attenuation mechanism, and therefore using another model did not result in any advantage. The resulting models were able to predict both NIR light and UV-VIS light attenuations accurately (R^2 over 0.965 and 0.850, respectively). Interestingly, the performance of the model decreased at low biomass concentrations (see Figure S14), with much better prediction capacities at concentrations above 500 g $COD_{biomass} \cdot m^{-3}$ (R^2 >0.994 for NIR spectrum and >0.980 for UV-VIS), which are frequently found in PPB systems (Capson-Tojo et al., 2020; Hülsen et al., 2018a). This is again related to the fact that the Lambert-Beer law can only account for light

28

absorption due to biomass, and thus at low biomass concentrations its prediction capabilities are jeopardised, as light absorption due to biomass loses relevance.

3.3.2. PAnM modification: light modelling in mechanistic models for PPB growth

Batch tests performed in anaerobic microplates were used to estimate the photoheterotrophic uptake rates at different light intensities (see Figure S15 for the experimental data). The corresponding values of $k_{M,I}$ are presented in Figure 5, together with a Monod function (Equation 1) fit to the data to predict the impact of light intensity on the photoheterotrophic uptake rates (the corresponding values of k_M and K_I are 2.65 ± 0.98 g COD·g COD^{-1}·d^{-1} and 4.58 ± 7.40 W·m^{-2}).

The maximum k_M value obtained is in agreement with the one used in the PAnM (2.65 ± 0.98 *vs.* 2.37 ± 0.40 g COD·g COD^{-1}·d^{-1}). Nevertheless, the half-saturation coefficient for light (intensity allowing an uptake rate equal to 50% of the maximum; K_I) differs considerably. While the value from our curve is 4.58 ± 7.40 W·m^{-2}, Puyol et al. (2017) used a K_I of 88 W·m^{-2} in the PAnM, a value that was gathered from the literature. The study where this value was taken from evaluated the effect of light intensity on hydrogen production, and 88 W·m^{-2} was the lowest tested intensity (Uyar et al., 2007). Although the authors reported a decrease in hydrogen production at 88 W·m^{-2} when compared to higher intensities, accurate K_I estimation would have required tests at lower intensities. In addition, the experimental design used did not account for light attenuation. It must be mentioned that the PAnM did not address the topic of light delivery in detail. In addition, the K_I value used in the PAnM (88 W·m^{-2}) was low enough to result in a process not limited by light (excluding attenuation, they assumed that the incident light intensity of 200-250 W·m^{-2} was constant throughout the whole reactor volume). The obtained uptake rates at low light intensities are also in agreement with values previously reported at 1.4-3.0 W·m^{-2}, of 1.37 g COD·g

COD^{-1}·d^{-1} (Dalaei et al., 2020).

The mechanistic PAnM from Puyol et al. (2017) was modified to include the uptake rates and the Monod function defined above (using I$_{ave}$ as light available for the biomass), as well as the Lambert-Beer equation obtained from the experiments using the flat plate reactor. Results from photoheterotrophic batch experiments (Capson-Tojo et al., 2021) were used for model validation. Both the simulation and the experimental results are presented in Figure 6. These show that the modified PAnM was able to accurately predict photoheterotrophic PPB growth, considering SCOD, inorganic N (IN), and inorganic P (IP) uptake. The values of the parameters used for the simulations can be found in Table S5. The Petersen matrix for this model is the same as the one reported in Puyol et al. (2017), and is therefore not presented here.

Figure 6 also shows the light intensity at different depths in the modelled reactors (for various batch times, *i.e.*, biomass concentrations). It can be observed that photoheterotrophic growth would have been limited considerably if a K$_l$ of 88 W·m^{-2} had been assumed, meaning that the kinetic constants previously used in the PAnM could not have represented the observed behaviour if attenuation had been considered. It has to be mentioned that, compared to the PAnM, the nitrogen and phosphorus contents in the biomass had to be modified to accurately predict the IN and IP profiles (from 0.086 g N·g COD$_{biomass}$$^{-1}$ and 0.015 g P·g COD$_{biomass}$$^{-1}$ to 0.065 g N·g COD$_{biomass}$$^{-1}$ and 0.010 g P·g COD$_{biomass}$$^{-1}$). The higher modelled final concentrations for IN and IP compared to the experimental results (see Figure 6) might be simply due to a slight overestimation of the biomass decay rates in the PAnM.

Due to the impact of the carotenoids and BChl concentrations on light attenuation, the possibility to include pigments as a state-variable in the model could be

considered, as in Wágner et al. (2018), which could be particularly interesting in aerated reactors, as dissolved oxygen impacts pigment availability. This was not considered in this work since the detailed analysis of PPB pigments is not available (and the overall concentrations are uniform under anaerobic conditions). Therefore, attenuation will depend mostly on biomass concentration. We note that very low illumination intensities might increase the pigment contents, but that these conditions would not be practical for wastewater treatment/resource recovery purposes (other than carotenoid production).

Finally, although the incident total light in the modelled indoor tests was lower than those used to estimate the attenuation coefficients (120 *vs.* 600-800 $W \cdot m^{-2}$), the influence of the incident light has been reported to be insignificant for attenuation purposes, particularly when the light source is distant from the illuminated surface or at high biomass concentrations (Naderi et al., 2017). The accurate modelling results confirmed the applicability of the used light attenuation functions.

3.4. Implications for industrial application

The results presented here show that light attenuation is a critical factor to be considered in PPB systems. Depending mostly on the biomass concentration and the light path (and therefore the reactor design), attenuation might lead to an insufficient light supply, limiting effective photoheterotrophic growth of PPB. Compared to other phototrophs, such as microalgae, the attenuation coefficients are similar for PPB (at a given biomass concentration). Nevertheless, it has to be considered that PPB reactors are expected to work at higher concentrations than microalgal systems, which will amplify the attenuation effect. Typical biomass concentrations in microalgae ponds treating wastewater rarely exceed 200-600 mg $VSS \cdot L^{-1}$, even when biomass retention is implemented (Robles et al., 2020a, 2020b; Wágner et al.,

31

2018). Since the biomass yield of PPB is around 1 g $COD_{biomass} \cdot g\ COD_{removed}^{-1}$, the biomass concentration in the reactors depends mostly on the concentration of biodegradable COD in the wastewater, which is commonly over 1.5-2.0 g $COD \cdot L^{-1}$ (*e.g.* in agri-industrial wastewaters), resulting in biomass concentrations over 1.0 g $VSS \cdot L^{-1}$ (Capson-Tojo et al., 2020; Hülsen et al., 2018b). In addition, NIR light absorption by water at low biomass concentration will also increase the attenuation effect in PPB systems (*e.g.*, for domestic wastewater treatment).

Maximising the treatment capacities and the biomass production rates is crucial to balance the high capital costs associated with outdoors PPB reactors (Capson-Tojo et al., 2020). This makes it imperative to provide optimal conditions for PPB growth, with uptake rates close to the maximum values. A light distribution allowing an effective photoheterotrophic growth is essential. Therefore, well-designed reactors/ponds must provide sufficient light along the light path, allowing effective PPB growth throughout the system to minimize dark zones. Figure 7 shows an example of maximum dimensions (*i.e.*, pond depth or flat plate width) that a PPB cultivation system could have to support 15 $W \cdot m^{-2}$ in all the reactor volume (15 $W \cdot m^{-2}$ was around the lowest intensity allowing maximum uptake rates, see Figure 5), under an illumination of 400 $W \cdot m^{-2}$ (NIR fraction; considered as a common value at zenith during winter months in sub-tropical areas (Kandilli and Ulgen, 2008)). The results show that the maximum depth of a pond working above 500 g $COD_{biomass} \cdot m^{-3}$ is below 5 cm, while a vertical flat plate reactor could have a thickness of around 10 cm, mainly due to the 2-sided illumination. These data suggest that common pond depths applied for microalgae systems (*e.g.*, over 20-30 cm) should not be extrapolated to PPB cultures, as no light would be available in most of the pond volume at these depths. These values are in agreement with recent results from an

open PPB pond, showing that a 10 cm deep raceway performed better than a system with a depth of 20 cm (Alloul et al., 2021). Heavy competition with non-phototrophic microbes would be expected in deep ponds, especially when considering that PPB systems are primed for raw wastewater (secondary rather than tertiary treatment) with sufficient COD. Minimising non-illuminated areas is a key factor in PPB-based systems, as the NIR-phototrophic capabilities are the main competitive advantage of PPB allowing their enrichment (as photoautotrophy in microalgae). Flat plate PBRs have recently been proposed as a promising option (Hülsen et al., 2022a, 2022b). Nevertheless, as PBRs are more expensive than open ponds, fully detailed economic analyses must be carried out before selecting one alternative over the other. Our results imply very large surfaces in ponds (even larger than for microalgae). At optimum water depths (*e.g.*, 5 cm), ponds would require very large surfaces and land areas, which in turn would increase oxygen diffusion, further disturbing the photoheterotrophic metabolism and increasing the competitiveness of common aerobic heterotrophs (Capson-Tojo et al., 2021). The alternative, *e.g.*, using common HRAP depths of around 30 cm, can be expected to result in a very diverse microbial population, where PPB might not be dominant due to the lack of light throughout most of the system. This would be indicated by low SCOD:N:P ratios and low biomass yields. However, in terms of oxygen diffusion, this might be a better alternative, as 5 cm deep PPB ponds might fail due to PPB outcompetition by faster growing common aerobic heterotrophs, especially if paddlewheel mixing is provided, thus increasing oxygen diffusion (Capson-Tojo et al., 2021). Research should be carried out regarding optimal design for ponds specific for PPB, continuing the work presented in Alloul et al. (2021).

Other than design and modelling purposes, the findings presented here are also

relevant for process optimisation. An example is the application of biomass retention in PPB reactors to increase the treatment capacities and volumetric production rates. This alternative has been previously applied, increasing significantly the biomass concentrations in the reactors and the treatment performances (Cerruti et al., 2020; Hülsen et al., 2016; Stegman et al., 2021). The results presented here show that the attenuation effect is increased at high biomass concentrations, which might hinder the application of biomass retention methods, unless the light path is optimised. Nevertheless, the asymptotic behaviour of the k_a values at biomass concentrations over 1.5-2.0 g $COD_{biomass} \cdot L^{-1}$ (see Figure 2) suggests that further increases in the biomass contents might not require significantly lower light path lengths to allow efficient photoheterotrophic operation.

4. Conclusions

PPB biomass attenuated both UV-VIS and NIR wavelengths, with an increasing fraction of UV-VIS at higher biomass concentrations. At concentrations above 1,000 mg $COD_{biomass} \cdot L^{-1}$ (≥ 600 g $VS \cdot m^{-3}$), the attenuation of both spectral bands was approximately equal. Light attenuation depended on the reactor configuration, with a square/rectangular cross-section attenuating less than a cylindrical cross-section. Attenuation was not impacted by the complexity of the wastewater matrix, or by the presence of PHA, but the concentration of pigments (both BChl and carotenoids) had a strong effect, likely related to their functionality as part of light harvesting complexes. Scattering had a minimal impact, as assessed by use of the Lambert-Beer equation *vs.* alternative models including light scattering. A proposed mathematical model, based on the Lambert-Beer law and a Monod function for light requirements, allowed effective representation of the kinetics of anaerobic

34

photoheterotrophic growth. The estimated half saturation coefficient for illumination was 4.6 $W \cdot m^{-2}$, indicating that non-incident irradiation can be an effective light source. The predicted NIR light penetration in outdoor PPB systems with biomass concentrations >1.0 $g \cdot L^{-1}$ is only 5 cm, which will favour engineered systems with multiple panels (*e.g.*, plate reactors), rather than horizontal lagoons.

Acknowledgements

Declaration **of** **interests**

The authors declare that they have no known competing financial interests or personal relationships that could have appeared to influence the work reported in this paper.

References

Acién Fernández, F.G., García Camacho, F., Sánchez Pérez, J.A., Fernández Sevilla, J.M., Molina Grima, E., 1997. A model for light distribution and average solar irradiance inside outdoor tubular photobioreactors for the microalgal mass culture. Biotechnol. Bioeng. 55, 701–714. https://doi.org/10.1002/(SICI)1097-0290(19970905)55:5<701::AID-BIT1>3.0.CO;2-F

Alloul, A., Cerruti, M., Adamczyk, D., Weissbrodt, D.G., Vlaeminck, S., 2021. Operational Strategies to Selectively Produce Purple Bacteria for Microbial Protein in Raceway Reactors. Environ. Sci. Technol. 55, 8278–8286.

https://doi.org/https://doi.org/10.1021/acs.est.0c08204

Anye Cho, B., Ross, B.S., du Toit, J.P., Pott, R.W.M.C., del Río Chanona, E.A., Zhang, D., 2021. Dynamic modelling of Rhodopseudomonas palustris biohydrogen production: Perturbation analysis and photobioreactor upscaling. Int. J. Hydrogen Energy 46, 36696–36708. https://doi.org/10.1016/j.ijhydene.2021.08.162

APHA, 2005. Standard Methods for the Examination of Water and Wastewater. American Public Health Association, Washington, DC.

Batstone, D.J., Keller, J., Angelidaki, I., Kalyuzhny, S. V, Pavlostathis, S.G., Rozzi, A., Sanders, W.T.M., Siegrist, H., Vavilin, V.A., 2002. Anaerobic digestion model no. 1 (ADM1). IWA Publishing. https://doi.org/https://doi.org/10.2166/wst.2002.0292

Batstone, D.J., Pind, P.F., Angelidaki, I., 2003. Kinetics of Thermophilic , Anaerobic Oxidation of Straight and Branched Chain Butyrate and Valerate. Biotechnol. Bioeng. 884, 195–204. https://doi.org/10.1002/bit.10753

Béchet, Q., Shilton, A., Guieysse, B., 2013. Modeling the effects of light and temperature on algae growth: State of the art and critical assessment for productivity prediction during outdoor cultivation. Biotechnol. Adv. 31, 1648–1663. https://doi.org/10.1016/j.biotechadv.2013.08.014

Bertie, J.E., Lan, Z., 1996. Infrared Intensities of Liquids XX: The Intensity of the OH Stretching Band of Liquid Water Revisited, and the Best Current Values of the Optical Constants of H_2O(l) at 25°C between 15,000 and 1 cm−1. Appl. Spectrosc. 50, 1047–1057. https://doi.org/10.1366/0003702963905385

Bolger, A.M., Lohse, M., Usadel, B., 2014. Trimmomatic: A flexible trimmer for Illumina sequence data. Bioinformatics 30, 2114–2120.

https://doi.org/10.1093/bioinformatics/btu170

Braun, C.L., Smirnov, S.N., 2020. WHY IS WATER BLUE? [WWW Document]. Dep. Chem. Dartmouth Coll. Hanover. URL https://web.nmsu.edu/~snsm/water/ (accessed 9.22.20).

Callahan, B.J., McMurdie, P.J., Rosen, M.J., Han, A.W., Johnson, A.J.A., Holmes, S.P., 2016. DADA2: High resolution sample inference from Illumina amplicon data. Nat. Methods 13, 581–583. https://doi.org/10.1038/nmeth.3869.DADA2

Canniffe, D.P., Hunter, C.N., 2014. Engineered biosynthesis of bacteriochlorophyll b in Rhodobacter sphaeroides. Biochim. Biophys. Acta - Bioenerg. 1837, 1611–1616. https://doi.org/10.1016/j.bbabio.2018.02.006

Caporaso, J.G., Kuczynski, J., Stombaugh, J., Bittinger, K., Bushman, F.D., Costello, E.K., Fierer, N., Peña, A.G., Goodrich, J.K., Gordon, J.I., Huttley, G.A., Kelley, S.T., Knights, D., Koenig, J.E., Ley, R.E., Lozupone, C.A., Mcdonald, D., Muegge, B.D., Pirrung, M., Reeder, J., Sevinsky, J.R., Turnbaugh, P.J., Walters, W.A., Widmann, J., Yatsunenko, T., Zaneveld, J., Knight, R., 2010. QIIME allows analysis of high- throughput community sequencing data Intensity normalization improves color calling in SOLiD sequencing. Nat. Methods 7, 335–336. https://doi.org/10.1038/nmeth0510-335

Capson-Tojo, G., Batstone, D.J., Grassino, M., Vlaeminck, S.E., Puyol, D., Verstraete, W., Kleerebezem, R., Oehmen, A., Ghimire, A., Pikaar, I., Lema, J.M., Hülsen, T., 2020. Purple phototrophic bacteria for resource recovery: Challenges and opportunities. Biotechnol. Adv. 43, 107567. https://doi.org/doi.org/10.1016/j.biotechadv.2020.107567

Capson-Tojo, G., Lin, S., Batstone, D.J., Hülsen, T., 2021. Purple phototrophic bacteria are outcompeted by aerobic heterotrophs in the presence of oxygen.

37

Water Res. 194, 116941. https://doi.org/10.1016/j.watres.2021.116941

Cerruti, M., Stevens, B., Ebrahimi, S., Alloul, A., 2020. Enrichment and Aggregation of Purple Non-sulfur Bacteria in a Photobioreactor for Biological Nutrient Removal From Wastewater. Front. Bioeng. Biotechnol. 8, 557234. https://doi.org/10.3389/fbioe.2020.557234

Cornet, J.F., Dussap, C.G., Dubertret, G., 1992. A structured model for simulation of cultures of the cyanobacterium Spirulina platensis in photobioreactors: I. Coupling between light transfer and growth kinetics. Biotechnol. Bioeng. 40, 817–825. https://doi.org/10.1002/bit.260400709

Dalaei, P., Bahreini, G., Nakhla, G., Santoro, D., Batstone, D., Hülsen, T., 2020. Municipal wastewater treatment by purple phototropic bacteria at low infrared irradiances using a photo-anaerobic membrane bioreactor. Water Res. 173, 115535. https://doi.org/10.1016/j.watres.2020.115535

De Vree, J.H., Bosma, R., Janssen, M., Barbosa, M.J., Wijffels, R.H., 2015. Comparison of four outdoor pilot-scale photobioreactors. Biotechnol. Biofuels 8, 1–12. https://doi.org/10.1186/s13068-015-0400-2

Engelbrektson, A., Kunin, V., Wrighton, K.C., Zvenigorodsky, N., Chen, F., Ochman, H., Hugenholtz, P., 2010. Experimental factors affecting PCR-based estimates of microbial species richness and evenness. ISME J. 4, 642–647. https://doi.org/10.1038/ismej.2009.153

Ghimire, A., Frunzo, L., Pirozzi, F., Trably, E., Escudie, R., Lens, P.N.L., Esposito, G., 2015. A review on dark fermentative biohydrogen production from organic biomass: Process parameters and use of by-products. Appl. Energy 144, 73–95. https://doi.org/10.1016/j.apenergy.2015.01.045

Grassino, M., Batstone, D.J., Yong, K.W.L., Capson-Tojo, G., Hülsen, T., 2022. A

method for detection and quantification of neurosporene, lycopene, and bacteriochlorophyll a in purple phototrophic bacteria by UPLC-UV-HRMS. Talanta Accepted w.

Gregor, J., Klug, G., 1999. Regulation of bacterial photosynthesis genes by oxygen and light. FEMS Microbiol. Lett. 179, 1–9. https://doi.org/10.1016/S0378-1097(99)00374-2

Henze, M., Gujer, W., Mino, T., van Loosdrecht, M.C.M., 2000. Activated Sludge Models ASM1, ASM2, ASM2d and ASM3. IWA Publishing.

Hülsen, T., Barry, E.M., Lu, Y., Puyol, D., Keller, J., Batstone, D.J., 2016. Domestic wastewater treatment with purple phototrophic bacteria using a novel continuous photo anaerobic membrane bioreactor. Water Res. 100, 486–495. https://doi.org/10.1016/j.watres.2016.04.061

Hülsen, T., Batstone, D.J., Keller, J., 2014. Phototrophic bacteria for nutrient recovery from domestic wastewater. Water Res. 50, 18–26. https://doi.org/10.1016/j.watres.2013.10.051

Hülsen, T., Hsieh, K., Lu, Y., Tait, S., Batstone, D.J., 2018a. Simultaneous treatment and single cell protein production from agri-industrial wastewaters using purple phototrophic bacteria or microalgae – A comparison. Bioresour. Technol. 254, 214–223. https://doi.org/10.1016/j.biortech.2018.01.032

Hülsen, T., Hsieh, K., Tait, S., Barry, E.M., Puyol, D., Batstone, D.J., 2018b. White and infrared light continuous photobioreactors for resource recovery from poultry processing wastewater – A comparison. Water Res. 144, 665–676. https://doi.org/10.1016/j.watres.2018.07.040

Hülsen, T., Stegman, S., Batstone, D.J., Capson-Tojo, G., 2022a. Naturally illuminated photobioreactors for resource recovery from piggery and chicken-

processing wastewaters utilising purple phototrophic bacteria. Water Res. 214, 118194. https://doi.org/doi.org/10.1016/j.watres.2022.118194

Hülsen, T., Züger, C., Batstone, D.J., Solley, D., Ochre, P., Porter, B., Capson-Tojo, G., 2022b. Outdoor demonstration-scale flat plate photobioreactor for resource recovery with purple phototrophic bacteria. Water Res. 216, 118327. https://doi.org/https://doi.org/10.1016/j.watres.2022.118327

IEA Bioenergy, 2017. State of Technology Review – Algae Bioenergy.

Jeppsson, U., Rosen, C., Alex, J., Copp, J., Gernaey, K. V., Pons, M.N., Vanrolleghem, P. a., 2006. Towards a benchmark simulation model for plant-wide control strategy performance evaluation of WWTPs. Water Sci. Technol. 53, 287–295. https://doi.org/10.2166/wst.2006.031

Kandilli, C., Ulgen, K., 2008. Solar illumination and estimating daylight availability of global solar irradiance. Energy Sources, Part A Recover. Util. Environ. Eff. 30, 1127–1140. https://doi.org/10.1080/15567030601100688

Lu, H., Zhang, G., Zheng, Z., Meng, F., Du, T., He, S., 2019. Bio-conversion of photosynthetic bacteria from non-toxic wastewater to realize wastewater treatment and bioresource recovery: A review. Bioresour. Technol. 278, 383–399. https://doi.org/10.1016/j.biortech.2019.01.070

Madigan, M.T., Martinko, J.M., Stahl, D.A., Clark, D.P., 2011. Bacteria: The Proteobacteria, in: 13th (Ed.), Brock Biology of Microorganisms. Pearson, pp. 477–480. https://doi.org/10.1038/hr.2014.17

Marsullo, M., Mian, A., Ensinas, A.V., Manente, G., Lazzaretto, A., Marechal, F., 2015. Dynamic modeling of the microalgae cultivation phase for energy production in open raceway ponds and flat panel photobioreactors. Front. Energy Res. 3, 1–18. https://doi.org/10.3389/fenrg.2015.00041

Masella, A.P., Bartram, A.K., Truszkowski, J.M., Brown, D.G., Neufeld, J.D., 2012. PANDAseq: PAired-eND Assembler for Illumina sequences. BMC Bioinformatics 13, 1–7.

Mavi, H.S., Tupper, G.J., 2004. Agrometeorology Principles and Applications of Climate Studies in Agriculture, 1st ed.

Molina Grima, E., Acien Fernandez, F.G., Garcia Camacho, F., Chisti, Y., 1999. Photobioreactors : light regime, mass transfer, and scaleup. J. Biotechnol. 70, 231–247.

Naderi, G., Znad, H., Tade, M.O., 2017. Investigating and modelling of light intensity distribution inside algal photobioreactor. Chem. Eng. Process. Process Intensif. 122, 530–537. https://doi.org/10.1016/j.cep.2017.04.014

Oehmen, A., Keller-Lehmann, B., Zeng, R.J., Yuan, Z., Keller, J., 2005. Optimisation of poly-β-hydroxyalkanoate analysis using gas chromatography for enhanced biological phosphorus removal systems. J. Chromatogr. A 1070, 131–136. https://doi.org/10.1016/j.chroma.2005.02.020

Okubo, Y., Futamata, H., Hiraishi, A., 2006. Characterization of phototrophic purple nonsulfur bacteria forming colored microbial mats in a swine wastewater ditch. Appl. Environ. Microbiol. 72, 6225–6233. https://doi.org/10.1128/AEM.00796-06

Ormerod, J.G., Ormerod, K.S., Gest, H., 1961. Light-Dependent Utilization of Organic Compounds and Photoproduction of Molecular bHydrogen by Photosynthetic Bacteria; Relationships with Nitrogen Metabolism. Arch. Biochem. Biophys. 94, 449–463.

Patton, C.J., Truitt, E.P., 1992. Methods of Analysis By the U.S. Geological Survey National Water Quality Laboratory—Determination of Total Phosphorus By a Kjeldahl Digestion Method and an Automated Colorimetric Finish That Includes

41

Dialysis. U.S. Geol. Surv. Open-File Rep. 92-146.

Pearson, W.R., Wood, T., Zhang, Z., Miller, W., 1997. Comparison of DNA sequences with protein sequences. Genomics 46, 24–36. https://doi.org/10.1006/geno.1997.4995

Pilon, L., Berberoĝlu, H., Kandilian, R., 2011. Radiation transfer in photobiological carbon dioxide fixation and fuel production by microalgae. J. Quant. Spectrosc. Radiat. Transf. 112, 2639–2660. https://doi.org/10.1016/j.jqsrt.2011.07.004

Posten, C., 2009. Design principles of photo-bioreactors for cultivation of microalgae. Eng. Life Sci. 9, 165–177. https://doi.org/10.1002/elsc.200900003

Puyol, D., Barry, E.M., Hülsen, T., Batstone, D.J., 2017. A mechanistic model for anaerobic phototrophs in domestic wastewater applications: Photo-anaerobic model (PAnM). Water Res. 116, 241–253. https://doi.org/10.1016/j.watres.2017.03.022

Quast, C., Pruesse, E., Yilmaz, P., Gerken, J., Schweer, T., Yarza, P., Peplies, J., Glöckner, F.O., 2013. The SILVA ribosomal RNA gene database project: Improved data processing and web-based tools. Nucleic Acids Res. 41, 590–596. https://doi.org/10.1093/nar/gks1219

Robles, Á., Capson-Tojo, G., Gales, A., Ruano, M.V., Sialve, B., Ferrer, J., Steyer, J., 2020a. Microalgae-bacteria consortia in high-rate ponds for treating urban wastewater : Elucidating the key state indicators under dynamic conditions. J. Environ. Manage. 261, 110244. https://doi.org/10.1016/j.jenvman.2020.110244

Robles, Á., Capson-Tojo, G., Gales, A., Viruela, A., Sialve, B., Seco, A., Steyer, J.-P., Ferrer, J., 2020b. Performance of a membrane-coupled high-rate algal pond for urban wastewater treatment at demonstration scale. Bioresour. Technol. 301, 122672. https://doi.org/10.1016/j.biortech.2019.122672

Ruivo, M., Cartaxana, P., Cardoso, M.I., Tenreiro, A., Tenreiro, R., Jesus, B., 2014. Extraction and quantification of pigments in aerobic anoxygenic phototrophic bacteria. Limnol. Oceanogr. Methods 12, 338–350. https://doi.org/10.4319/lom.2014.12.338

Ruiz-Martínez, A., Serralta, J., Seco, A., Ferrer, J., 2016. Modeling light and temperature influence on ammonium removal by Scenedesmus sp. under outdoor conditions. Water Sci. Technol. 74, 1964–1970. https://doi.org/10.2166/wst.2016.383

Saer, R.G., Blankenship, R.E., 2017. Light harvesting in phototrophic bacteria: Structure and function. Biochem. J. 474, 2107–2131. https://doi.org/10.1042/BCJ20160753

Sganga, M.W., Bauer, C.E., 1992. Regulatory factors controlling photosynthetic reaction center and light-harvesting gene expression in Rhodobacter capsulatus. Cell 68, 945–954. https://doi.org/10.1016/0092-8674(92)90037-D

Stegman, S., Batstone, D.J., Rozendal, R., Jensen, P.D., Hülsen, T., 2021. Purple phototrophic bacteria granules under high and low upflow velocities. Water Res. 190, 116760. https://doi.org/10.1016/j.watres.2020.116760

Uyar, B., Eroglu, I., Yücel, M., Gündüz, U., Türker, L., 2007. Effect of light intensity, wavelength and illumination protocol on hydrogen production in photobioreactors. Int. J. Hydrogen Energy 32, 4670–4677. https://doi.org/10.1016/j.ijhydene.2007.07.002

Wágner, D.S., Valverde-Pérez, B., Plósz, B.G., 2018. Light attenuation in photobioreactors and algal pigmentation under different growth conditions – Model identification and complexity assessment. Algal Res. 35, 488–499. https://doi.org/10.1016/j.algal.2018.08.019

Wágner, D.S., Valverde-Pérez, B., Sæbø, M., Bregua de la Sotilla, M., Van Wagenen, J., Smets, B.F., Plósz, B.G., 2016. Towards a consensus-based biokinetic model for green microalgae – The ASM-A. Water Res. 103, 485–499. https://doi.org/10.1016/j.watres.2016.07.026

Yu, S., Xu, Y., Liang, C., Lou, W., Peng, L., 2022. Spectral bands of incandescent lamp leading to variable productivity of purple bacteria biomass and microbial protein: Full is better than segmented. Sci. Total Environ. 823, 153736. https://doi.org/10.1016/j.scitotenv.2022.153736

Zhu, Y.S., Cook, D.N., Leach, F., Armstrong, G.A., Alberti, M., Hearst, J.E., 1986. Oxygen-regulated mRNAs for light-harvesting and reaction center complexes and for bacteriochlorophyll and carotenoid biosynthesis in Rhodobacter capsulatus during the shift from anaerobic to aerobic growth. J. Bacteriol. 168, 1180–1188. https://doi.org/10.1128/jb.168.3.1180-1188.1986

Figure and table captions

Figure 1. (A) NIR and (B) UV-VIS attenuation curves for the 6 L cylindrical reactor at different biomass concentrations (g COD·m^{-3}), and the (C) NIR fraction in the measured light.

Figure 2. Dependence of the attenuation coefficients from the Lambert-Beer law (k_a) on the biomass concentration. Different reactor configurations are shown, separating (A) NIR and (B) UV-VIS wavelengths. Both experimental and modelling results (data fit to a power function) for the different configurations is shown (R^2 of 0.990-0.999). The error bars represent 95% confidence intervals. For comparison purposes, values for microalgae are also presented (from Wágner et al. (2018), assuming a conversion factor of 1.6 g COD·g TSS^{-1}).

44

Figure 3. Effective attenuation coefficients for (A) NIR and (B) UV-VIS spectra, calculated as the product of the attenuation coefficient (k_a) and the biomass concentration (X_{PB}), at increasing X_{PB} values. The error bars represent 95% confidence intervals.

Figure 4. Dependence of the (left) NIR and (right) UV-VIS attenuation coefficients from the Lambert-Beer law (ka) on the biomass concentration for the experiments using (A, B) PWWTE, (C, D) PHA-enriched cultures, and (E, F) non-pigmented biomass (*vs.* pigmented). The error bars represent 95% confidence intervals.
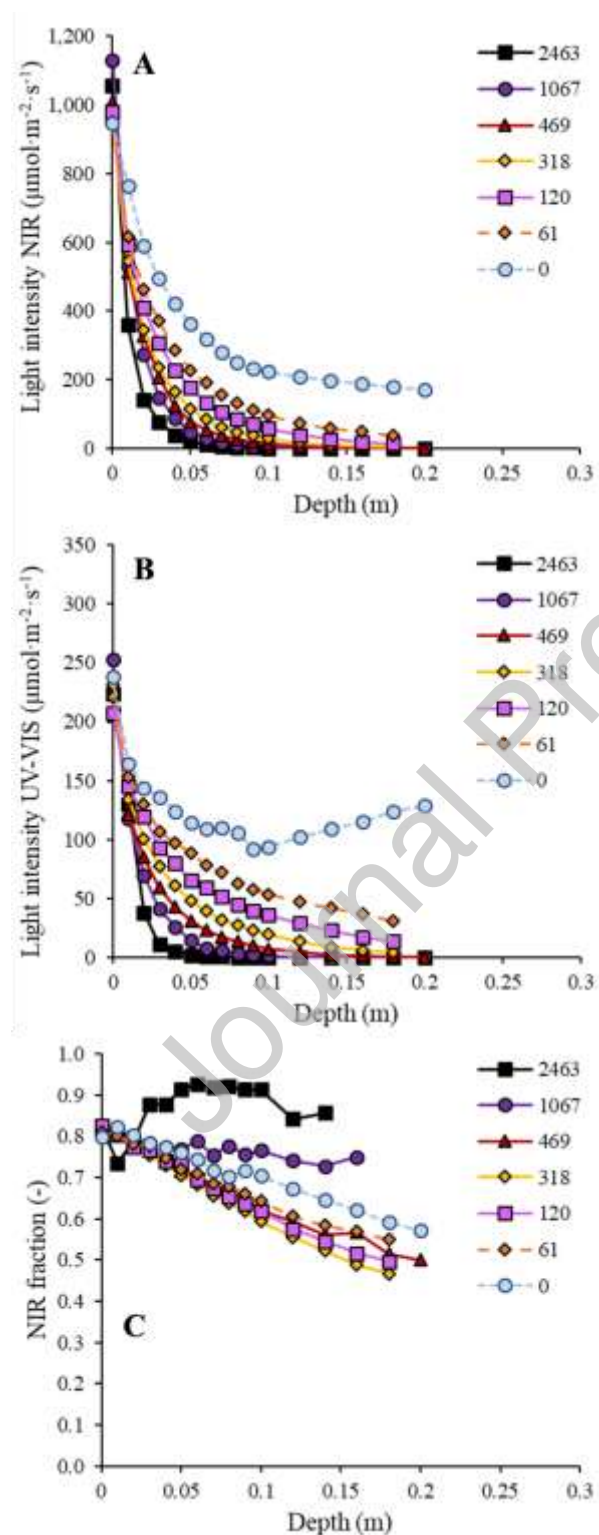
Figure 5 (A) Estimated photoheterotrophic uptakes rates (k_M) of acetate at different light intensities and corresponding modelled values using a Monod function. (B) Parameter determination results including 95% confidence intervals and confidence regions. The error bars represent 95% confidences intervals in mean.

Figure 6. Experimental and modelled results of the photoheterotrophic batch test used for model validation (R^2 values of 0.97-0.98). The predicted light attenuation profiles at different times of the batch test (times given in days) are also shown. SCOD stands for soluble chemical demand, IN for inorganic nitrogen, IP for inorganic phosphorus, and IZ for the light intensity at a given depth z.

Figure 7. Maximum dimensions (light path length) allowing a minimum light intensity of 15 W·m^{-2} in all the reactor volume, assuming an incident NIR light of 400 W·m^{-2}. The values are given for different biomass concentrations and reactor configurations.

**Table 1.** Kinetic parameters of a power function to describe the attenuation coefficients (k_a; m^2·g COD^{-1}) as a function of the biomass concentration (X_{PB}; g COD·m^{-3}).

45

Table 2. Parameters and performance of the different attenuation models for the experiments using different reactors (NIR light).
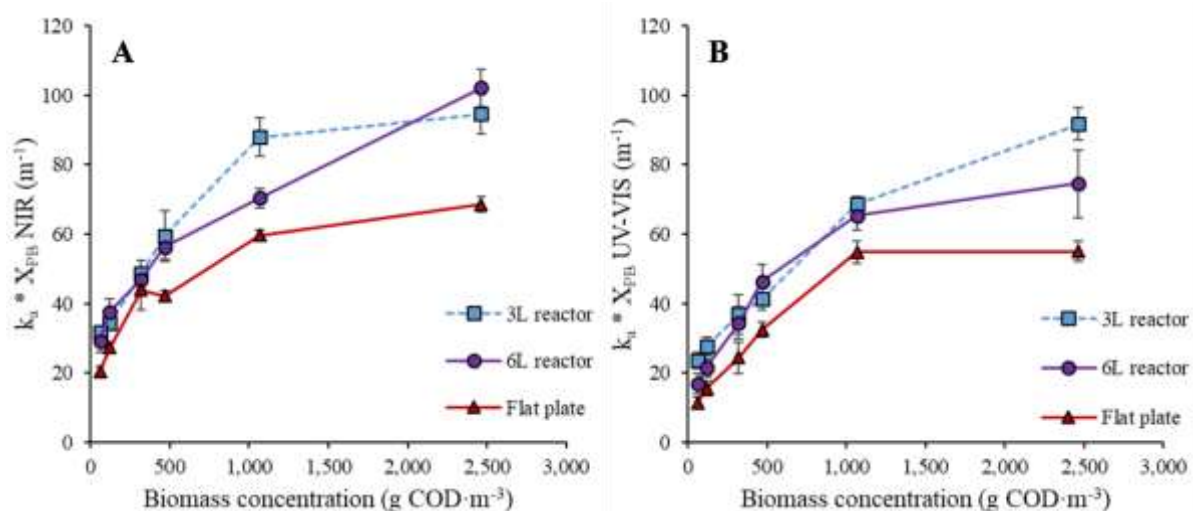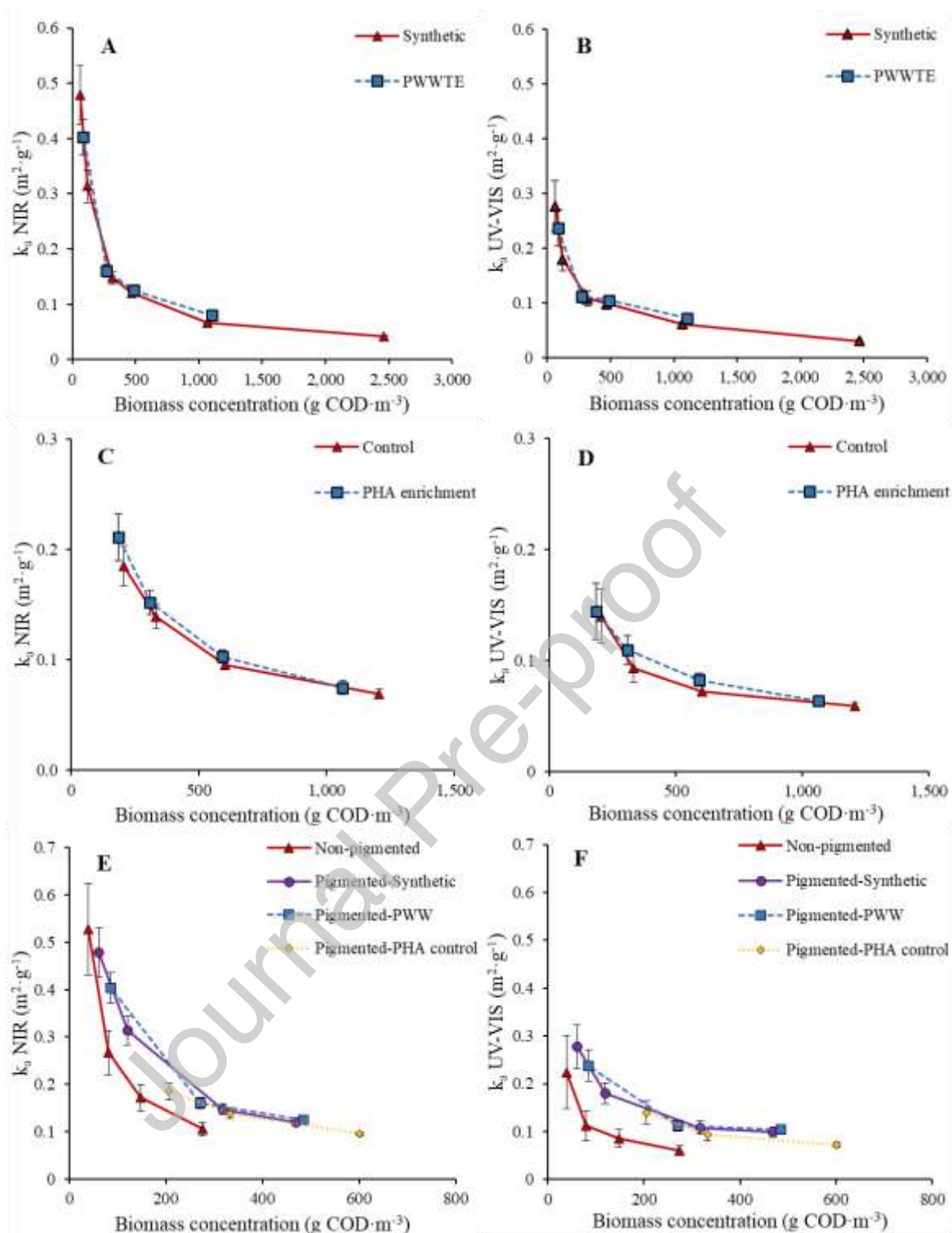
Figure 1. (A) NIR and (B) UV-VIS attenuation curves for the 6 L cylindrical reactor at different biomass concentrations (g COD·m^{-3}), and (C) NIR fraction in the measured light.
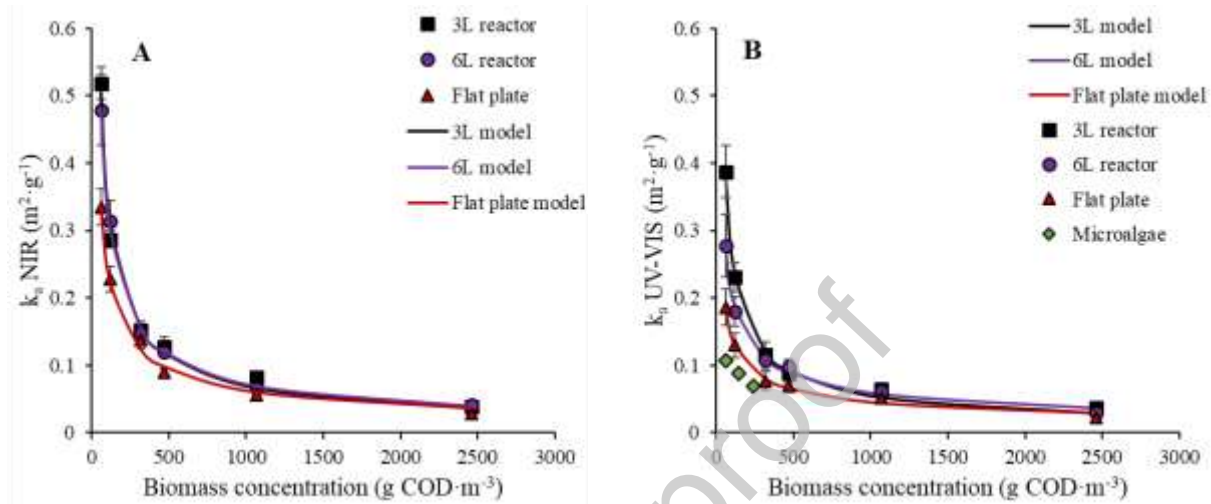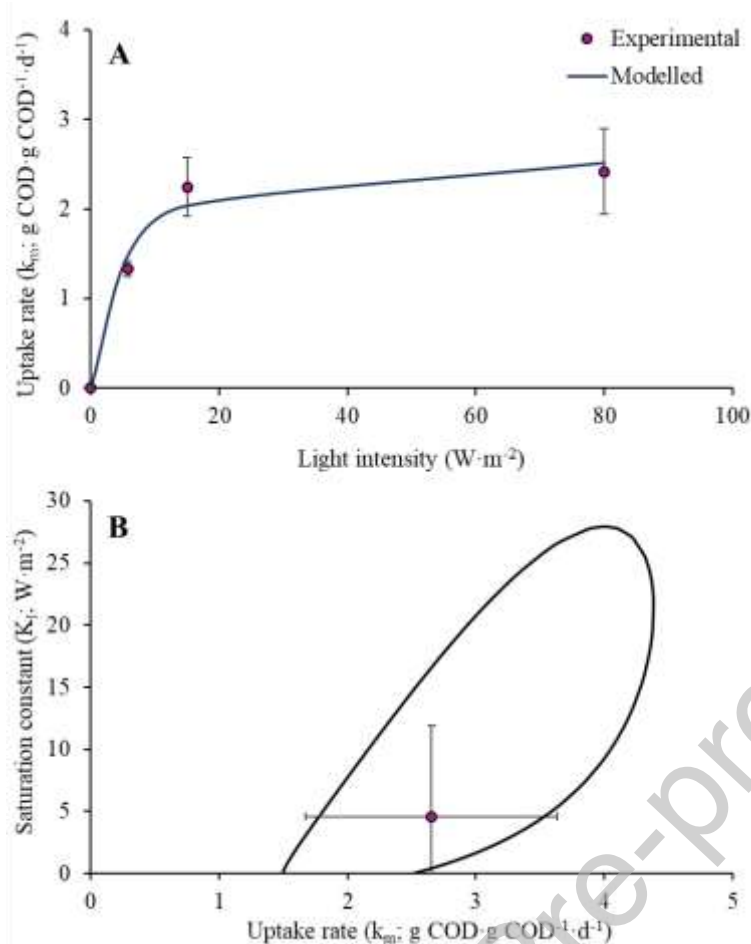

Figure 2. Dependence of the attenuation coefficients from the Lambert-Beer law (k$_a$) on the biomass concentration. Different reactor configurations are shown, separating (A) NIR and (B) UV-VIS wavelengths. Both experimental and modelling results (data fit to a power function) for the different configurations is shown (R^2 of 0.990-0.999). The error bars represent 95% confidence intervals. For comparison purposes, values for microalgae are also presented (from Wágner et al. (2018), assuming a conversion factor of 1.6 g COD·g TSS^{-1}).
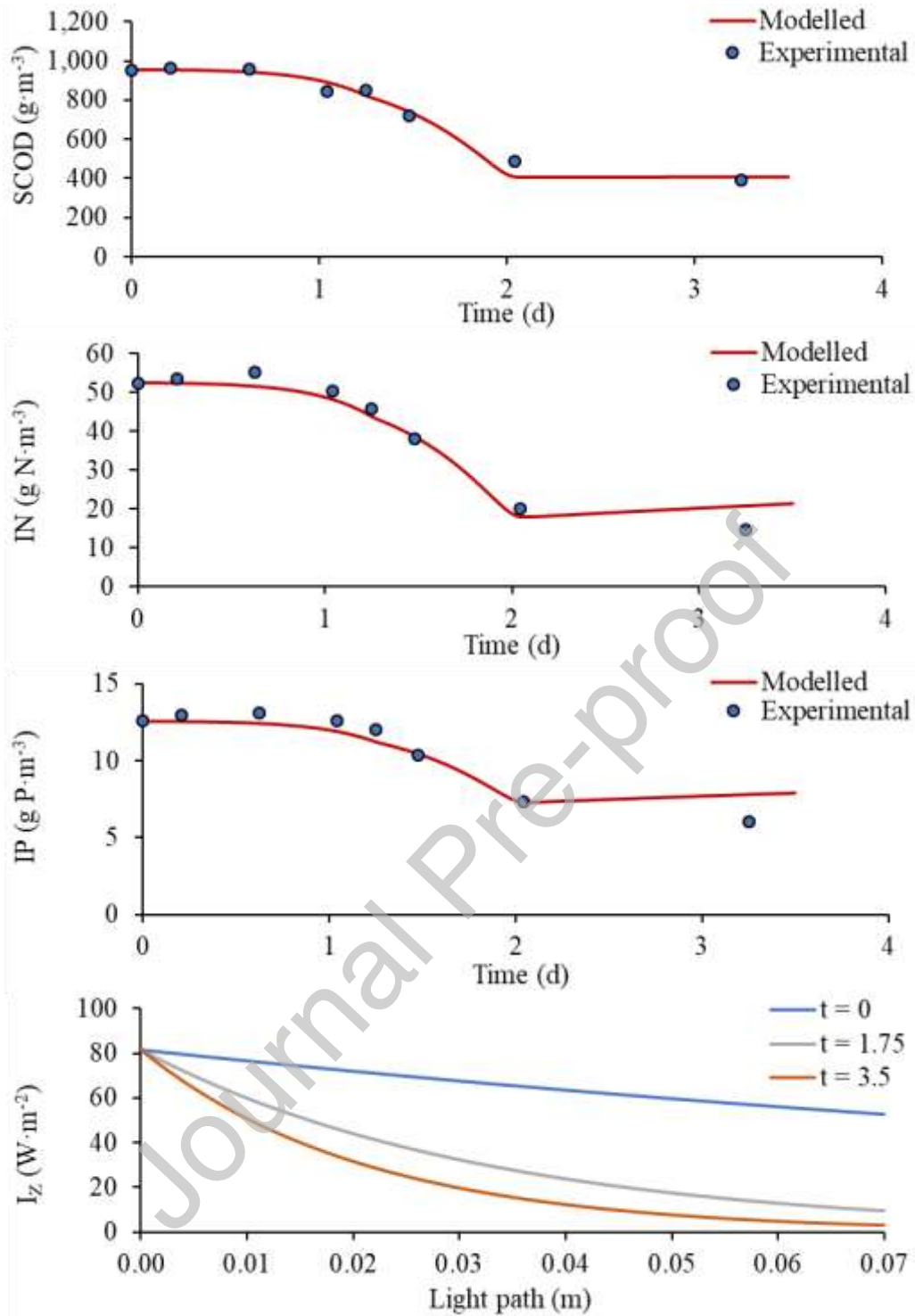
Figure 3. Effective attenuation coefficients for (A) NIR and (B) UV-VIS spectra, calculated as the product of the attenuation coefficient (k_a) and the biomass concentration (X_{PB}), at increasing X_{PB} values. The error bars represent 95% confidence intervals.

48

Figure 4. Dependence of the (left) NIR and (right) UV-VIS attenuation coefficients from the Lambert-Beer law (k_a) on the biomass concentration for the experiments using (A, B) PWWTE, (C, D) PHA-enriched cultures, and (E, F) non-pigmented biomass (*vs.* pigmented). The error bars represent 95% confidence intervals.
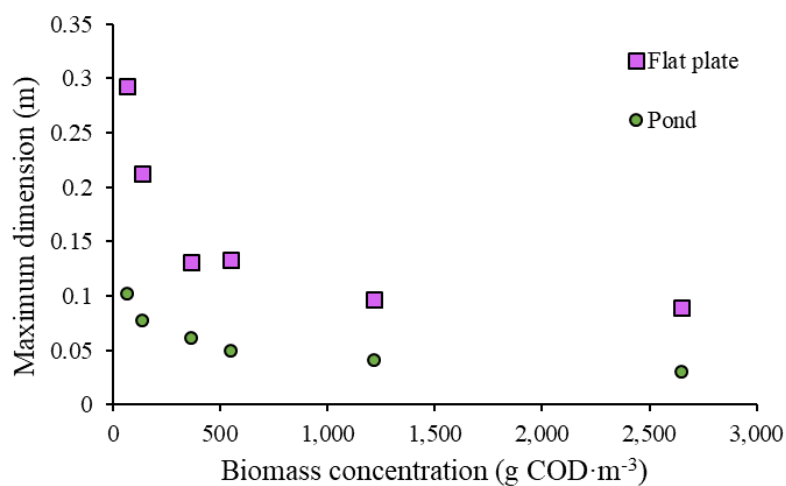
49

Figure 5. (A) Estimated photoheterotrophic uptakes rates (k_M) of acetate at different light intensities and corresponding modelled values using a Monod function. (B) Parameter determination results including 95% confidence intervals and confidence regions. The error bars represent 95% confidences intervals in mean.

Figure 6. Experimental and modelled results of the photoheterotrophic batch test used for model validation (R^2 values of 0.97-0.98). The predicted light attenuation profiles at different times of the batch test (times given in days) are also shown. SCOD stands for soluble chemical demand, IN for inorganic nitrogen, IP for inorganic

phosphorus, and I_z for the light intensity at a given depth z.

Figure 7. Maximum dimensions (light path length) allowing a minimum light intensity

of 15 W·m^{-2} in all the reactor volume, assuming an incident NIR light of 400 W·m^{-2}.

The values are given for different biomass concentrations and reactor configurations.

Table 1. Kinetic parameters of a power function to describe the attenuation coefficients (k_a; $m^2 \cdot g\ COD^{-1}$) as a function of the biomass concentration (X_{PB}; g $COD \cdot m^{-3}$).

Light spectrum	Reactor	a ($m^5 \cdot g^{-2}$)	b (-)	R^2
NIR	Cylindrical (6 L)	8.00 ± 1.76	0.68 ± 0.05	0.9986
	Cylindrical (3 L)	9.30 ± 5.60	0.71 ± 0.13	0.9901
	Flat plate	4.09 ± 1.54	0.61 ± 0.08	0.9946
UV-VIS	Cylindrical (6 L)	2.59 ± 0.90	0.55 ± 0.07	0.9940
	Cylindrical (3 L)	6.58 ± 2.93	0.69 ± 0.10	0.9943
	Flat plate	1.47 ± 0.51	0.51 ± 0.07	0.9927
NIR	Global fit	6.93 ± 3.98	0.67 ± 0.12	0.9352
UV-VIS	Global fit	3.22 ± 2.72	0.59 ± 0.19	0.8255

Table 2. Parameters and performance of the different attenuation models for the experiments using different reactors (NIR light).

Reactor	Light spectrum	Biomass concentration (g COD·m⁻³)	Lambert-Beer		Schuster			Hyperbolic		
			k_a (m²·g COD⁻¹)	R^2	E_a (m²·g COD⁻¹)	E_s (m²·g COD⁻¹)	R^2	At_{max} (m⁻¹)	K_{at} (g COD·m⁻³)	R^2
Cylindrical (6 L)	NIR	2463	0.041 ± 0.002	0.9981	0.041 ± 0.003	$5 \cdot 10^{-10}$ ± 0.004	0.9981	102 ± 0	0.990 ± 0.599	0.9981
		1067	0.066 ± 0.002	0.9985	0.066 ± 0.004	$8 \cdot 10^{-11}$ ± 0.006	0.9985	70.5 ± 0	0.990 ± 0.916	0.9985
		469	0.120 ± 0.008	0.9946	0.120 ± 0.012	$7 \cdot 10^{-10}$ ± 0.021	0.9946	56.4 ± 0	0.990 ± 1.24	0.9946
		318	0.148 ± 0.011	0.9920	0.148 ± 0.018	$1 \cdot 10^{-9}$ ± 0.032	0.9920	47.1 ± 0	0.990 ± 1.42	0.9920
		120	0.314 ± 0.030	0.9821	0.314 ± 0.054	$3 \cdot 10^{-9}$ ±0.098	0.9821	38.0 ± 0	0.990 ± 2.20	0.9821
		61	0.478 ± 0.053	0.9692	0.478 ± 0.099	$2 \cdot 10^{-9}$ ± 0.187	0.9692	29.7 ± 0	0.990 ± 2.78	0.9692
Cylindrical (3 L)	NIR	2463	0.038 ± 0.002	0.9971	0.038 ± 0.003	$5 \cdot 10^{-9}$ ± 0.005	0.9971	94.7 ± 0	0.990 ± 0.591	0.9971
		1067	0.082 ± 0.005	0.9964	0.082 ± 0.007	$1 \cdot 10^{-9}$ ± 0.011	0.9964	88.0 ± 0	0.990 ± 0.805	0.9964
		469	0.127 ± 0.016	0.9800	0.127 ± 0.025	$9 \cdot 10^{-10}$ ± 0.042	0.9800	59.6 ± 0	0.990 ± 1.19	0.9800
		318	0.153 ± 0.012	0.9899	0.153 ± 0.021	$2 \cdot 10^{-9}$ ± 0.036	0.9899	48.7 ± 0	0.990 ± 1.34	0.9899
		120	0.287 ± 0.012	0.9960	0.287 ± 0.023	$2 \cdot 10^{-9}$ ± 0.042	0.9960	34.7 ± 0	0.990 ± 1.94	0.9960
		61	0.518 ± 0.024	0.9952	0.518 ± 0.045	$8 \cdot 10^{-9}$ ± 0.083	0.9952	32.1 ± 0	0.990 ± 2.68	0.9952
Flat plate	NIR	2463	0.028 ± 0.001	0.9998	0.028 ± 0.001	$8 \cdot 10^{-14}$ ± 0.001	0.9998	68.6 ± 0	0.990 ± 0.638	0.9998
		1067	0.056 ± 0.001	0.9997	0.056 ± 0.002	$4 \cdot 10^{-10}$ ± 0.003	0.9997	59.7 ± 0	0.934 ± 0.945	0.9997
		469	0.090 ± 0.003	0.9989	0.090 ± 0.005	$2 \cdot 10^{-12}$ ± 0.009	0.9989	42.3 ± 0	0.990 ± 1.18	0.9989
		318	0.138 ± 0.018	0.9885	0.138 ± 0.028	$1 \cdot 10^{-9}$ ± 0.044	0.9885	44.1 ± 0	0.990 ± 1.69	0.9885
		120	0.228 ± 0.013	0.9967	0.228 ± 0.022	$2 \cdot 10^{-9}$ ± 0.040	0.9967	27.6 ± 0	0.990 ± 2.29	0.9967
		61	0.335 ± 0.025	0.9936	0.335 ± 0.043	$2 \cdot 10^{-8}$ ± 0.078	0.9936	20.7 ± 0	0.990 ± 2.77	0.9936

54